UCSF

UC San Francisco Previously Published Works

Title

A Cell-Penetrating Scorpion Toxin Enables Mode-Specific Modulation of TRPA1 and Pain

Permalink

https://escholarship.org/uc/item/6ns5b34n

Journal

Cell, 178(6)

ISSN

0092-8674

Authors

Lin King, John V

Emrick, Joshua J

Kelly, Mark JS

et al.

Publication Date

2019-09-01

DOI

10.1016/j.cell.2019.07.014

Peer reviewed

eScholarship.org Powered by the California Digital Library
University of California

Author Manuscript

Author Manuscript

Author Manuscript

Author Manuscript

HHS Public Access

Author manuscript

Cell. Author manuscript; available in PMC 2020 September 05.

Published in final edited form as:

Cell. 2019 September 05; 178(6): 1362–1374.e16. doi:10.1016/j.cell.2019.07.014.

A cell-penetrating scorpion toxin enables mode-specific modulation of TRPA1 and pain

John V. Lin King[1,2], **Joshua J. Emrick**[1,3,†], **Mark J.S. Kelly**[4], **Volker Herzig**[5], **Glenn F. King**[5], **Katalin F. Medzihradszky**[4,‡], **David Julius**[1,6,*]

[1]Department of Physiology, University of California, San Francisco; San Francisco, California, 94143; United States of America

[2]Neuroscience Graduate Program, University of California, San Francisco; San Francisco, California, 94143; United States of America

[3]Oral and Craniofacial Sciences Program, School of Dentistry, University of California; San Francisco, California, 94143; United States of America

[4]Department of Pharmaceutical Chemistry, University of California, San Francisco; San Francisco, California, 94143; United States of America

[5]Institute for Molecular Bioscience, University of Queensland; St. Lucia, Queensland, 4072; Australia

[6]Lead Contact

Summary

TRPA1 is a chemosensory ion channel that functions as a sentinel for structurally diverse electrophilic irritants. Channel activation occurs through an unusual mechanism involving covalent modification of cysteine residues clustered within an amino-terminal cytoplasmic domain. Here we describe a peptidergic scorpion toxin (WaTx) that activates TRPA1 by penetrating the plasma membrane to access the same intracellular site modified by reactive electrophiles. WaTx stabilizes TRPA1 in a biophysically distinct active state characterized by prolonged channel openings and low Ca^{2+} permeability. Consequently, WaTx elicits acute pain and pain hypersensitivity, but fails to trigger efferent release of neuropeptides and neurogenic inflammation typically produced by noxious electrophiles. These findings provide a striking example of convergent evolution whereby

*Correspondence: david.julius@ucsf.edu.

†Present address: National Institute of Dental and Craniofacial Research, National Institutes of Health; Bethesda, Maryland, 20892; United States of America

‡Present address: Laboratory of Proteomics Research, Biological Research Centre of the Hungarian Academy of Sciences; Szeged, 6727; Hungary

Author Contributions J.V.L.K. and D.J. conceived and designed the project; J.V.L.K. carried out all experiments and analyzed results with collaborative contributions and guidance on behavioral (J.J.E.), NMR (M.J.S.K.), and mass spectrometry (K.F.M.) studies. V.H. and G.F.K. contributed the invertebrate venom library and *U. manicatus* venom. J.V.L.K. and D.J. wrote the paper, with input from all authors.

Publisher's Disclaimer: This is a PDF file of an unedited manuscript that has been accepted for publication. As a service to our customers we are providing this early version of the manuscript. The manuscript will undergo copyediting, typesetting, and review of the resulting proof before it is published in its final citable form. Please note that during the production process errors may be discovered which could affect the content, and all legal disclaimers that apply to the journal pertain.

Declaration of Interests The authors declare no competing interests.

Author Manuscript Author Manuscript Author Manuscript Author Manuscript

chemically disparate animal- and plant-derived irritants target the same key allosteric regulatory site to differentially modulate channel activity. WaTx is a unique pharmacological probe for dissecting TRPA1 function and its contribution to acute and persistent pain.

Graphical Abstract

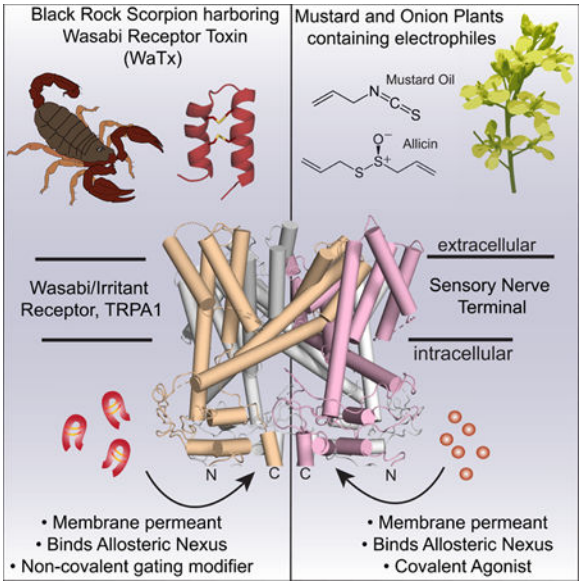

In Brief

A selective cell-penetrating scorpion toxin targets the irritant receptor, TRPA1, via a distinct biochemical mechanism than that used by irritants, allowing definition of a new mechanism of channel activation and interrogation of pathways of pain sensitization.

Introduction

The TRPA1 ion channel (also known as the wasabi receptor) is expressed by primary afferent sensory neurons, where its activation by piquant natural products from mustard and allium plants elicits the sinus clearing or eye stinging pain one experiences when eating wasabi or chopping an onion (Bandell et al., 2004; Jordt et al., 2004). This reflects TRPA1's role as a chemosensory receptor for a broad class of volatile environmental irritants and endogenous inflammatory agents that directly activate the channel to produce acute and persistent pain. TRPA1 also functions as a 'receptor-operated' channel that is activated downstream of phospholipase C-coupled receptors that detect pruritic and pro-inflammatory agents (Bandell et al., 2004; Bautista et al., 2006). Thus, TRPA1 is considered a promising therapeutic target for treating chronic pain, itch and neurogenic inflammatory syndromes that are initiated or exacerbated by nociceptor activation (Andersson et al., 2008; Bautista et al., 2013; Julius, 2013).

Most TRPA1 agonists, including plant-derived irritants, environmental toxicants, and endogenous products of oxidative stress, are chemically reactive electrophiles (*e.g.* isothiocyanates, thiosulfinates and α, β-unsaturated aldehydes) that work through a unique

Author Manuscript Author Manuscript Author Manuscript Author Manuscript

mechanism involving covalent modification of specific cysteine residues located within the channel's cytoplasmic amino terminus (Bahia et al., 2016; Hinman et al., 2006; Macpherson et al., 2007). A recent cryo-EM structure of TRPA1 localized these modification sites to an intricately folded intracellular domain termed the 'allosteric nexus.' This reflects the idea that this locus constitutes a key regulatory site for stimulus integration that is poised to propagate ligand-evoked conformational changes to the channel's gate (Bahia et al., 2016; Palovcak et al., 2015; Paulsen et al., 2015).

Natural, non-electrophilic TRPA1 agonists have been identified, such as Δ9-tetrahydrocannabinol (THC) and menthol. However, these compounds are of low potency, efficacy, and specificity, limiting their usefulness as probes for understanding non-covalent mechanisms of TRPA1 activation (Jordt et al., 2004; Karashima et al., 2007). We therefore wondered whether other non-chemically reactive TRPA1 ligands exist and, if so, do their mechanisms of action elicit distinct biophysical, physiologic, and behavioral responses. Identifying such pharmacophores and their mechanisms of action is essential to fully understanding and manipulating TRPA1 function under normal (acute) and pathophysiological (chronic) pain states. Indeed, a critical goal in developing novel analgesics is to modulate the activity of key receptors or channels in the context of chronic pain while sparing their core protective functions – a challenge that has beset d evelopment of drugs targeting the heat / capsaicin receptor, TRPV1 (Basbaum et al., 2009; Moran, 2018).

To begin to address this important issue in regard to TRPA1, we turned to animal venoms as evolutionarily honed chemical 'libraries' that cont ain pain-inducing defensive agents (Bohlen et al., 2011; Bohlen and Julius, 2012; Hille, 2001; Osteen et al., 2016; Siemens et al., 2006; Zhang et al., 2017). While hundreds of peptide toxins are known to target voltage-gated ion channels, few have been identified that act on TRP channels, and these all activate the capsaicin receptor, TRPV1 (Bohlen et al., 2010; Hille, 2001; Kalia et al., 2015; King and Hardy, 2013; Siemens et al., 2006). Despite the similarly prominent role of TRPA1 in nociception and pain, algogenic toxins targeting this member of the TRP channel family have not been described.

Here we identify a potent and selective peptide scorpion toxin that modulates TRPA1 by crossing the plasma membrane and binding to the same allosteric nexus that is covalently modified by electrophilic irritants. In doing so, the toxin stabilizes a unique channel state characterized prolonged open times and low divalent cation permeability, which we exploit to elucidate the contribution of intrinsic TRPA1 calcium permeability to efferent nociceptor function, neurogenic inflammation, and pain hypersensitivity.

Results

Black Rock scorpions produce a TRPA1-activating toxin

We used ratiometric calcium (Ca^{2+}) imaging of rat TRPA1-expressing HEK293T (HEK) cells to screen through a large invertebrate venom library in search of direct channel activators. Because TRPA1 is activated by manipulations that increase intracellular free Ca^{2+} (Jordt et al., 2004; Wang et al., 2008), high throughput screening of crude venoms (which

Author Manuscript Author Manuscript Author Manuscript Author Manuscript

contain a multitude of proteases, lipases, and other hydrolytic activities) can be plagued by false positives (Bohlen and Julius, 2012). We therefore began our search by first depleting venoms of high molecular weight cell-lytic components, and by instituting a counter-screen in which intracellular Ca^{2+} stores were depleted prior to venom addition (Jordt et al., 2004; Osteen et al., 2016; Zhang et al., 2017). In this way, we zeroed in on venom from the Australian Black Rock scorpion (*Urodacus manicatus*, (Thorell, 1876)) as containing a robust TRPA1 activator (Figure 1A,B; S1A–C). Reversed phase HPLC yielded a single active peptide whose primary amino acid sequence was determined by manual interpretation of high resolution, high mass accuracy collision-induced dissociation mass spectra (Figure 1C; S1D, E, G; Table S1). The deduced pattern of cysteine residues suggested a 1–4, 2–3 arrangement of disulfide bonds (Figure 1C) (Quintero-Hernandez et al., 2013; Tytgat et al., 1999). Indeed, a cognate synthetic peptide with this same arrangement fully recapitulated activity of the native species and was used for all further experiments (Figure S1F).

We first asked if this peptide, which we call Wasabi Receptor Toxin (WaTx), constitutes a potent, direct, and selective TRPA1 ligand. Application of WaTx to human TRPA1-transfected HEK cells produced characteristic outwardly rectifying membrane currents that reversed rapidly upon toxin washout when compared with those evoked by the covalent electrophilic agonist, mustard oil (allyl isothiocyanate, AITC) (τ_{off} = 4.6 ± 1.2 vs. 27 ± 5 seconds for WaTx and AITC, respectively; $p < 0.05$, unpaired two-tailed Student's *t*-test). Toxin-evoked responses were blocked by the TRPA1-selective channel inhibitor, A 967079 (Figure 1D–F) (Chen et al., 2011), and did not require extracellular or intracellular Ca^{2+}, indicative of direct toxin action on the channel (Figure 1D). Furthermore, recordings were carried out in nominally Ca^{2+}-free bath solution when intracellular Ca^{2+} was chelated with EGTA, demonstrating that these responses do not require extracellular or intracellular Ca^{2+}. These observations are consistent with direct action of the toxin on TRPA1 (Figure 1D). WaTx was both potent (EC_{50} = 15, 95% CI 13–18 nM) and selective since application of a saturating dose (5μM) of toxin to trigeminal sensory neurons from wild-type mice excited only the cohort sensitive to a selective dose of AITC (50μM). Furthermore, WaTx had no effect on neurons from TRPA1-deficient animals (Figure 1G, H; S1H–L). To further test toxin specificity, we asked whether WaTx elicited effects on other heterologously expressed sensory TRP channels or representative members of classical voltage-gated potassium channel subfamilies (Shaker, Shal, Shab, and Shaw). We observed neither inhibition nor enhancement of channel activity when toxin was applied alone (at concentrations saturating for TRPA1) or in combination with a relevant stimulus (Figure S1C, M, N).

Membrane penetration is required for WaTx action

In contrast to classic TRPA1 agonists, WaTx is a relatively large macromolecule that lacks any obvious electrophilic character. We therefore initiated a series of patch clamp recording experiments to probe its mechanism and site of action. At the outset, we were surprised to observe WaTx-evoked responses in the on-cell patch configuration, prior to rupturing the membrane to achieve whole-cell access (Figure S2A). This suggested that WaTx mediates its effect either by generating a cytoplasmic second messenger, or by crossing the membrane to access TRPA1 channels under the patch pipette (Horn, 1991; Lipscombe et al., 1989; Sakmann and Neher, 2009). To distinguish between these possibilities, we asked whether the

Author Manuscript Author Manuscript Author Manuscript Author Manuscript

toxin elicited responses when applied to membranes excised from the cell in an outside-out or inside-out configuration. Remarkably, activity was observed in either configuration, consistent with a membrane penetrating mechanism of WaTx action (Figure 2A, B; S2 B, C). To test this idea directly, we established a FRET-based assay to quantify translocation of fluorescently tagged WaTx into liposomes loaded with an acceptor fluorophore coupled to IgG. This reductionist, cell-free system allowed us to quantitatively and kinetically assess peptide movement across a lipid bilayer. Indeed, toxin readily crossed the liposome bilayer with a rate-constant linearly related to concentration, reaching equilibrium within minutes (Figure 2D, E).

WaTx bears little sequence homology to other known peptides, although its disulfide bonding pattern is reminiscent of a small family of κ-KTx scorpion toxins that form cysteine-stabilized helical hairpins (Cs α/α), or spider and crab toxins that form a cysteine-stabilized antiparallel β-sheet (Cs β/β) (Quintero-Hernandez et al., 2013; Silva et al., 2000; Srinivasan et al., 2002) (Figure 1C). Moreover, WaTx bears no obvious sequence similarity to classical cell penetrating peptides (CPPs), such as HIV Tat or *Drosophila* penetratin (Derossi et al., 1994; Frankel and Pabo, 1988; Joliot et al., 1991; Kauffman et al., 2015; Vives et al., 1997). To identify WaTx features that might enable membrane penetration, we determined its atomic structure using solution NMR (Figure S2H–K; Table S2). We found the toxin adopts a rigid and compact helical hairpin fold stabilized by two disulfide bonds (Figure 2C; S2K), consistent with its resemblance to κ-KTx scorpion toxins. A patch or preponderance of basic residues has previously been associated with cell-penetrating properties of peptides (Guidotti et al., 2017; Kauffman et al., 2015). In this regard, a notable tertiary structural feature of WaTx is the formation of a basic patch at the open end of the hairpin, where amino- and carboxy-termini meet. Here, the amino-terminal helix exhibits an unusually dense (4.5σ) dipole moment (Felder et al., 2007). Together, these features may constitute the cell penetrating motif (Figure 2F).

To test this hypothesis, we evaluated toxins bearing alanine substitution at four residues (K7, Q4, Q5, and R32) within this basic patch for their ability to activate TRPA1 in cell-attached versus excised inside-out configurations. Of these, only K7A displayed a reduced ability to activate channels in cell-attached mode, even though it was fully functional when applied to excised patches (Figure 2G; S2D–I). Consistent with these data, we observed ~25% reduction in the rate at which this mutant was able to load liposomes (Figure 2E), suggesting that this basic residue is important for facilitating membrane penetration. Altogether, these results support a direct mechanism of peptide penetration *via* passive diffusion (Bechara and Sagan, 2013; Guidotti et al., 2017; Kauffman et al., 2015) and establish that cell penetration and channel activation are distinct biophysical properties of the toxin.

WaTx targets the intracellular allosteric nexus of TRPA1

The ability of WaTx to penetrate the membrane does not *a priori* limit its site of action to an intracellular domain, and we therefore set out to identify its site of action using physiological and biochemical assays. TRPA1 orthologues show significant phylogenetic variation (Cordero-Morales et al., 2011; Gracheva et al., 2010; Kang et al., 2010; Kindt et al., 2007; Prober et al., 2008), and we indeed found that mammalian TRPA1 orthologues are

Author Manuscript Author Manuscript Author Manuscript Author Manuscript

activated by WaTx, whereas channels from more distantly related species (such as snakes, fish, flies and worms) are insensitive (Figure 3A; S3A, B). We leveraged this differential profile to initiate an unbiased, chimeric receptor approach to identify a region of TRPA1 that specifies toxin sensitivity, using human and rat snake TRPA1 (hTRPA1 and rsTRPA1, respectively) as the donor-recipient pair (Figure 3A; S3B, C, K). Transfer of the C-terminal TRP domain from rat snake to human TRPA1 produced a channel that was insensitive to WaTx but robustly activated by AITC, implicating this domain as a key element in specifying toxin sensitivity (Figure S3C). However, the inverse chimera (rsTRPA1 harboring the human TRP domain) remained toxin insensitive, indicating that this region is necessary, but insufficient to confer WaTx sensitivity (Figure S3D). In the three-dimensional structure of TRPA1, the TRP domain engages in extensive interactions with the N-terminal, cysteine-rich linker domain, an interaction that forms the core of the ‘allosteric nexus’ that is critical for activation by electrophilic agonists. Indeed, we found that transfer of the cysteine-rich linker region from the human to rat snake channel was sufficient to confer toxin sensitivity (Figure S3D). Within the cysteine-rich linker, conversion of three amino acids of the human channel (hTPRA1 P622A, M634L, and T646P) to cognate rat snake residues abrogated toxin sensitivity (Figure 3B, C; S3E–G). Of the converse changes, only the first (rsTRPA1 A627P) was sufficient to confer toxin sensitivity to the rat snake channel, demonstrating that a proline in this position is a key determinant of WaTx species selectivity (Figure 3C, D and G; S3H, J).

To ask whether the allosteric nexus forms a binding site for the toxin, we established a biolayer interferometry-based assay in which immobilized, biotinylated WaTx was used to capture crude membranes containing TRPA1. In this way we measured WaTx:TRPA1 interaction directly. Robust binding was observed with membranes prepared from hTRPA1- but not rsTRPA1-transfected HEK293 cells (Figure 3E, F; S3I). Importantly, membranes containing the rsTRPA1 gain-of-function mutant (A627P) did display binding, while those containing the hTPRA1 loss-of-function mutant (P622A) did not, consistent with their electrophysiological profiles (Figure 3A–F; S3I). From these data, we determined an off-rate constant for WaTx binding to hTRPA1 (k_{off} = 4.28 ± 0.39 ± 10^{-4} min^{-1}) and a conservative estimate of a dissociation constant (k_{on} = 8.80 10^9 ± 0.59 ± 10^9 mol^{-1} min^{-1}; K_D = 0.33 ± 0.55 pM) (Figure 3E). Taken together, these results demonstrate that WaTx binds directly and tightly to TRPA1, likely involving interactions with an integrated complex formed between the N-terminal cysteine-rich linker and C-terminal TRP domains. We propose that this binding site is located at subunit interfaces where the three-dimensional structure shows that these regions are in close apposition and form a potential binding pocket in which the toxin could nestle (Figure 3G, H) (Paulsen et al., 2015). In either case, our results show that WaTx acts at the structurally integrated allosteric nexus that also transduces electrophile reactivity to the channel gate.

WaTx stabilizes a unique channel open state

If electrophiles and WaTx converge on a single TRPA1 domain to activate the channel, do they work through similar or distinct biophysical mechanisms? Neither agent altered the voltage-dependence of channel activation, although close inspection revealed dramatically different kinetics of toxin-versus electrophile-evoked tail currents, suggesting distinct

Author Manuscript Author Manuscript Author Manuscript Author Manuscript

mechanisms of action (Figure S4A–C). Indeed, each agent also had strikingly different effects on single channel behavior. AITC elicited a large increase in open probability characterized by brief (≤ 5 msec) transitions between open and closed states (Figure 4A, B; S4D). Moreover, AITC application dramatically shortened the average latency to first channel opening, consistent with behavior of a true agonist that directly promotes channel opening (Figure 4C; S4E). On the other hand, WaTx produced openings that were markedly longer (≤ 20 msec.), and with an average latency to first opening that was indistinguishable from that of basal, spontaneous events (Figure 4A–C; S4E). Thus, in contrast to AITC, WaTx behaves as a gating modifier that stabilizes, rather than directly promotes the open state.

The differential effects of electrophile and toxin on gating can be further illustrated by the finding that WaTx reversibly modifies constitutively active channels. We demonstrated this by first eliciting channel openings by brief application of the irreversible electrophilic agonist, iodoacetamide (IAM) (Hinman et al., 2006). Following IAM washout, exposure to WaTx reversibly shifted the distribution of open state dwell times rightward (τ_{dwell} = 1.5 ± < 0.01 and 2.8 ± 0.6 msec. for IAM and WaTx, respectively; $p < 0.0001$, unpaired two-tailed Student's *t*-test) (Figure 4D, E). These results reinforce the notion that WaTx specifically modulates the TRPA1 open state and demonstrate that the actions of electrophiles and WaTx are functionally distinct and not mutually exclusive.

While these ligands produce kinetically distinguishable open states, do these states also differ with respect to ion conductance or permeability (Chung et al., 2008; Tominaga et al., 1998)? To address this question, we determined ion permeability sequences of hTRPA1 during spontaneous, AITC- or WaTx-evoked openings. These measurements were carried out with excised membrane patches from hTRPA1-transfected HEK cells to afford complete control over 'extracellular' and 'intracellular' cations, in par ticular Ca^{2+} (Bobkov et al., 2011; Wang et al., 2008). In excellent agreement with previous reports, TRPA1 displayed notable (~ 8 fold) selectivity for divalent over monovalent cations; was impermeant to the large organic cation NMDG; and, when stimulated with AITC, produced a small but significant increase in divalent cation selectivity (Figure 4F, S4F, G) (Bobkov et al., 2011; Karashima et al., 2010; Nagata et al., 2005; Story et al., 2003). Surprisingly, however, WaTx largely abolished the channel's preference for divalent over monovalent cations (Figure 4F; S4F, G), suggesting that it produces a unique open configuration of the ion conduction pathway. In contrast to these differential effects on ion selectivity, neither ligand altered Ca^{2+} conductance, and Na^{+} conductance was potentiated when Ca^{2+} was present at the channel's cytoplasmic face (Figure 4F, S4G), as previously described (Wang et al., 2008). These findings, including differential effects of electrophiles versus WaTx on open state kinetics and cation permeability, were also observed with mouse TRPA1 (Figure S4H–J). Taken together, our results demonstrate that spontaneous, electrophile- and toxin-evoked open states are kinetically and functionally distinct.

WaTx produces pain hypersensitivity without inflammation

AITC and other electrophiles excite TRPA1-positive, peptidergic nociceptors to elicit acute pain and neurogenic inflammation that is accompanied by hypersensitivity to thermal and

Author Manuscript Author Manuscript Author Manuscript Author Manuscript

mechanical stimuli (Basbaum et al., 2009; Bautista et al., 2006; Bautista et al., 2013). In light of the observed biophysical differences between WaTx- and electrophile-mediated TRPA1 activation, we asked whether these agents elicit the same spectrum of algogenic responses.

Like AITC, WaTx injection into the mouse hindpaw produced vigorous, dose-dependent nocifensive (pain-related) behavior that engaged central nociceptive neuronal pathways, as evidenced by induction of c-Fos immunoreactivity in superficial laminae of the spinal cord dorsal horn (Figure 5A–C; S5A–C). These responses were not observed in TRPA1-deficient mice, demonstrating toxin specificity *in vivo* (Figure 5A–C; S5B, C).

Intraplantar AITC injection elicited characteristic paw swelling and increased vascular permeability, responses that underlie neurogenic inflammation resulting from TRPA1-evoked vesicular release of pro-inflammatory neuropeptides (Substance P and CGRP). Surprisingly, while WaTx evoked acute pain behavior, it failed to produce these key signatures of neurogenic inflammation (Figure 5F, G; S5D). Consistent with this differential physiologic response, AITC promoted robust CGRP release from cultured rat trigeminal neurons, while WaTx did not (Figure 5H). This release occurred in the presence of voltage-gated Ca^{2+} channel inhibitors, but not when TRPA1 was blocked or intracellular Ca^{2+} chelated, demonstrating its dependence on Ca^{2+} entry through TRPA1 *per se* (Figure S5K). Thus, we conclude that WaTx fails to promote CGRP release (and thus neurogenic inflammation) because it reduces Ca^{2+} permeability of activated TRPA1 channels compared to electrophiles. Indeed, WaTx was able to promote CGRP release from cultured sensory neurons when the driving force for Ca^{2+}entry was increased by raising extracellular Ca^{2+} levels 10-fold (Figure 5H). Taken together, these results demonstrate that high intrinsic Ca^{2+} permeability is critical to the role that TRPA1 normally plays in post-injury neurogenic inflammatory responses that ideally promote recovery, but which can also become pathological.

Despite this robust and unexpected difference in local edema, both AITC and WaTx produced substantial and long-lasting hypersensitivity to thermal and mechanical stimuli (Figure 5D, E; S6E). Presumably, in the absence of peripheral inflammation, the toxin drives pain hypersensitivity primarily through a centrally-mediated mechanism. Because most TRPA1-positive sensory neurons also express the capsaicin receptor, TRPV1, we could ablate synaptic connections between TRPA1-expressing nerve fibers and the spinal cord by injecting capsaicin into the intrathecal (spinal) canal. While this manipulation ablates the central terminals of these neurons, their peripheral terminals are preserved and still capable of releasing inflammatory peptides (Figure S5G) (Cavanaugh et al., 2009; Emrick et al., 2018). Indeed, in such animals, injection of AITC into the paw produced swelling, but not acute nocifensive behavior (Figure S5H–J). Furthermore, these animals developed mechanical hypersensitivity (albeit with a delayed onset) that is likely produced when TRPV1/TRPA1-negative sensory fibers are activated by peripheral inflammation (Figure 5E). When capsaicin-ablated animals were treated with WaTx, they also lacked acute nocifensive behavior, but failed to exhibit any signs of mechanical hypersensitivity (Figure 5E), consistent with a predominantly central mechanism of toxin-evoked sensitization. Thus,

Author Manuscript Author Manuscript Author Manuscript Author Manuscript

WaTx pharmacologically isolates the central component of TRPA1-mediated pain hypersensitivity, reflecting its ability to elicit mode-specific channel gating.

Discussion

TRP channels are complex polymodal signal detectors that are capable of integrating information from physical and/or chemical stimuli to modulate cell excitability in the face of changing environmental or physiological conditions (Clapham, 2003; Latorre et al., 2009; Venkatachalam and Montell, 2007). In the context of the primary afferent nociceptor, this concept has great significance for understanding how tissue injury and inflammation produce pain hypersensitivity (Bautista et al., 2013; Julius, 2013). The capsaicin receptor, TRPV1, has served as a model for delineating biophysical and structural underpinnings of polymodality, reflecting the channel's rich pharmacology and the availability of numerous structurally and functionally distinct activators (heat, extracellular protons, bioactive lipids, pungent vanilloids, and peptide toxins) with which to probe these mechanisms (Basbaum et al., 2009; Julius, 2013). TRPA1 also plays a key role in nociception and inflammatory pain, but a comparative dearth of pharmacological tools has limited our understanding of the physiological and biophysical complexity of this channel, and thus potential strategies for controlling its function (Nilius et al., 2011). The identification of WaTx as a chemically and mechanistically novel TRPA1 activator helps to fill this gap. Indeed, we have exploited this toxin to identify a previously unrecognized open state of the channel that elicits distinct physiological and behavioral outcomes, providing proof-of-principle that the allosteric nexus of TRPA1 can be pharmacologically targeted to tune channel activity in a manner more subtle than previously appreciated, which may have therapeutic value.

Scorpions produce a TRP channel toxin

Scorpiones represent the most ancient extant source of arachnid venoms. These creatures are best known for deploying α and β–type toxins that target voltage-gated sodium and potassium channels for offense and defense (Bosmans and Tytgat, 2007; Kalia et al., 2015; Quintero-Hernandez et al., 2013), but have not previously been appreciated to deploy TRP channel toxins. Our analysis of WaTx species selectivity (Figure S3A) suggests that the Black Rock scorpion has evolved this toxin for the defensive purpose of deterring mammalian predators, rather than subduing invertebrate prey. WaTx belongs to a small, enigmatic family of orphan scorpion toxins (κ-KTx), whose name derives from the finding that one such toxin (Hefutoxin, κ-KTx1.1) functions as a low affinity blocker of cloned *Shaker* type potassium channels. However, *bona fide* physiological targets and mechanisms of action for this or other κ-KTx family members remain unknown (Quintero-Hernandez et al., 2013; Srinivasan et al., 2002). Our findings now pinpoint a high affinity physiologic target for one such compact, cysteine-stabilized helical-hairpin toxin. This broadens our view of the potential pharmacological properties and applications for members of this toxin family, which share a common fold but little sequence similarity.

WaTx is a novel cell-penetrating peptide

Peptide toxins are generally assumed to bind to extracellular domains of their protein targets, which in many cases likely involves partial penetration of the toxin into the membrane and

Author Manuscript Author Manuscript Author Manuscript Author Manuscript

formation of stabilizing interactions with lipids in the outer leaflet of the bilayer (Gao et al., 2016; Hille, 2001; Jung et al., 2005; Lee and MacKinnon, 2004; Mihailescu et al., 2014). WaTx takes this process to the extreme by fully translocating across the bilayer to access a cytoplasmic binding site on TRPA1. Mechanism underlying membrane translocation by polycationic peptides remain debated (Bechara and Sagan, 2013; Guidotti et al., 2017; Kauffman et al., 2015). Specifically, much attention has been paid to the question of whether such peptides translocate passively or are taken up by energy-dependent cellular processes (*e.g.*, endocytosis). Our experiments with excised membrane patches and liposomes support a passive penetration mechanism for WaTx, which likely constitutes the rate-limiting step for target engagement and channel activation (Figures 1G; 2D, E; and 3E).

Many CPPs, such as the HIV transactivator (Tat) or a fly Antennapedia homeoprotein-derived peptide (penetratin), lack well defined tertiary structure, but possess features that have been implicated in their cell penetrating properties, including overall hydrophobic or amphipathic character and/or the presence of cationic patches (Guidotti et al., 2017; Heitz et al., 2009; Joliot and Prochiantz, 2004). WaTx adopts a highly ordered and stable tertiary fold that forms a basic patch and dipole element that we implicate in cell penetration, providing a new model for studying the properties of passively translocating CPPs. While Maurocalcin, another highly structured scorpion toxin of the inhibitor-cysteine-knot type, also accumulates in cells to target the ER-localized ryanodine receptor, its penetration mechanism remains poorly understood and may involve both energy-dependent and independent processes (Quintero-Hernandez et al., 2013). In any case, our findings raise the intriguing possibility that other members of the κ-KTx family (or other highly structured peptide toxins) are adept at cell penetration and represent new pharmacological probes for identifying and manipulating intracellular sites on receptors, channels, or other targets.

The ‘allosteric nexus’ controls TRPA1 gating

WaTx and wasabi provide a striking example of convergent evolution wherein structurally dissimilar animal- and plant-derived irritants target the same domain to modulate TRPA1. In the case of WaTx, this evolutionary pathway reflects the ‘solution’ of two challenges: recognizing a key control point on TRPA1 and crossing the plasma to interact with this site. Furthermore, our results show that TRPA1’s allosteric nexus can function as a polymodal detector of diverse physiologic stimuli, including covalent and non-covalent ligands. This stands in contrast to TRPV1, where plant-derived vanilloids bind to a pocket deep within the bilayer, whereas spider toxins bind to the extracellular domain of the channel, likely reflecting the importance of these distinct regions for detecting physiologically relevant TRPV1 modulators, such as bioactive lipids and extracellular protons, respectively (Bohlen et al., 2010; Siemens et al., 2006)

While electrophiles and WaTx converge on a common site, they act through distinct mechanisms: covalent modification by electrophiles increases the probability of channel opening, whereas non-covalent WaTx binding stabilizes the open state and prolongs open time, reminiscent of the differential actions of benzodiazepines and barbiturates on $GABA_A$ receptors, which target non-overlapping sites on the same channel subunit to enhance open probability or mean open time, respectively—properties that underl ie the distinct clinical

Author Manuscript Author Manuscript Author Manuscript Author Manuscript

utilities of these allosteric modulators (Nicoll et al., 1975; Twyman et al., 1989). In this same vein, understanding the precise structural basis of WaTx and electrophile action may provide important insights into the function of the allosteric nexus and how this region of TRPA1 can be pharmacologically exploited to produce physiologically (and perhaps therapeutically) distinct outcomes.

TRPA1 Ca^{2+} *permeability, peptide release, and pain*

One notable characteristic of WaTx-evoked responses is the substantially reduced permeability of TRPA1 to Ca^{2+} ions. This observation suggests that the toxin and electrophiles stabilize distinct conformations of the gate and/or selectivity filter. Indeed, similar observations have been made for TRPV1 when comparing heat- and capsaicin-evoked currents (Chung et al., 2008; Tominaga et al., 1998), possibly reflecting the conformationally dynamic nature of the outer pore domain and associated selectivity filter (Bohlen et al., 2010; Cao et al., 2013; Gao et al., 2016; Liao et al., 2013). Our finding that TRPA1 also exhibits profound changes in ion selectivity suggests that these domains may likewise be conformationally dynamic and participate in both ion selectivity and channel gating. In the case of TRPV1, the ability to visualize these conformational changes was greatly facilitated by the discovery of DkTx and other gating modifier spider toxins (Bohlen et al., 2010; Cao et al., 2013; Gao et al., 2016; Liao et al., 2013) WaTx may similarly help stabilize key conformational states for future structural studies that reveal TRPA1 gating and permeation mechanisms, and how the ‘allosteric nexus’ controls these key channel functions.

While many TRP channels, such as TRPV1 and TRPA1, pass both mono- and divalent cations (and exhibit unusually high permeability for the latter), the relative contribution of these ionic species to physiological responses has been difficult to parse. Here we have been able to exploit the differential effects of AITC and WaTx to show that Ca^{2+} entry through this channel *per se* is both necessary and sufficient to initiate neurogenic inflammation by promoting release of pro-inflammatory peptides from activated peripheral nociceptor terminals. In contrast, bulk cation current flow through TRPA1 in response to either agent is sufficient to depolarize the neuron and transmit information to the spinal cord to evoke acute and persistent pain (Figure 6). This differential activity has enabled us to unmask the central component of TRPA1-evoked pain hypersensitivity without the confounding contributions from peripheral inflammation, making WaTx a unique tool for future mechanistic studies of central neural pathways contributing to chronic pain. Moreover, further insights into the structural basis of WaTx action may suggest strategies for targeting the allosteric nexus to diminish the inflammatory component of TRPA1-mediated pain while preserving its acute protective role in chemo-nociception.

STAR METHODS

LEAD CONTACT AND MATERIALS AVAILABILITY

Further information and requests for resources and reagents should be directed to and will be fulfilled by the lead contact, David Julius (david.julius@ucsf.edu). These include plasmids described in this study and synthetic peptides, the latter depending upon laboratory stocks.

Author Manuscript Author Manuscript Author Manuscript Author Manuscript

EXPERIMENTAL MODEL AND SUBJECT DETAILS

Molecular biology and cell culture—We used Full-length wild-type human TRPA1 and Texas rat snake TRPA1 (*Elaphe obsoleta lindheimeri*; GenBank ID: GU562966) subcloned into the mammalian/oocyte expression vector pMO for all experiments (Cordero-Morales et al., 2011; Gracheva et al., 2010). We designed TRPA1 chimaeras such that the junction points consisted of amino acid sequences conserved between the two orthologs (Figure S4K). Genscript (Nanjing, Jiangsu, CN) produced and verified all TRPA1 chimaeras and point mutants.

We cultured HEK (ATCC) cells at 37 ° C, 5% CO_2 in DMEM Complete (DMEM-C; Dulbecco's modified Eagle's medium containing 10% (v/v) heat-inactivated calf serum, 100 U ml^{-1} Penicillin G and 0.1 mg ml^{-1} Streptomycin). For heterologous expression of ion channels, we transfected cells with 0.25–1 μg of plasmid DNA combined with 3x (w/w) Lipofectamine 2000 (Thermo-Fisher) for 4–8 hrs. in Opti-MEM (Thermo Fisher) before plating onto coverslips with (for excised patch experiments and Ca^{2+-}-imaging experiments) or without (for all other experiments) 0.01% poly-L-Lysine (poly-L, MW 70–150,000, MilliporeSigma).

For analysis of WaTx effects in sensory neurons, we harvested trigeminal ganglia from early postnatal (P0–4) Sprague-Dawley rat or C57BL/6J mouse pups, digested them in Collagenase (1 mg ml^{-1}) followed by Trypsin (0.25% w/v) at 37 ° C for 15 min. each. We then mechanically triturated digested ganglia in DMEM-C, then plated neurons onto coverslips coated with poly-L and 10 μg ml^{-1} mouse laminin (PLL). Neurons were cultured for > 12 hrs. before use, under identical culture conditions to HEK cells.

Animal husbandry—Mice and rats were housed them at a density of 2–5 individuals/cage and 12 hr. light/dark cycle had *ad libitum* access to food and water. We conducted all animal care and behavioral experimentation in accordance with UCSF Institutional Animal Care Committee guidelines, the National Institutes of Health Guide of Care and Use of Laboratory Animals, and the recommendation of the International Association for the Study of Pain. In this study, adult (12–28 week-old) C57BL/6J mice (Jackson Laboratories) constituted the "wild-type" group and homozygous TRPA1 knockout mice on a C57BL/6J background constituted the "TRPA1 $^{-/-}$" group. (Bautista et al., 2006)

METHOD DETAILS

Venom library screening—We prepared and screened ~100 invertebrate venoms, as described previously (Osteen et al., 2016). Briefly, we filtered *U. manicatus* venom with a 50 kDa MWCO filter (MilliporeSigma) to remove high molecular weight cell-lytic components (Zhang et al., 2017) and to buffer-exchange into Ringer's solution containing, in mM, 140 NaCl, 10 HEPES, 5 KCl, 2 $MgCl_2$, 2 $CaCl_2$, and 10 Glucose; pH 7.4 with NaOH; 290–300 mOsm kg^{-1}. We then performed ratiometric Ca^{2+}-imaging (described below) of HEK293T (HEK) cells stably expressing TRPA1 or TRPM8 (McNamara et al., 2007).

WaTx Cloning—We purified WaTx from approximately 1 mg of crude *U. manicatus* venom via reverse-phase HPLC on an analytical monomeric Grace Vydac C_{18} column

Author Manuscript Author Manuscript Author Manuscript Author Manuscript

(300Å pore; I.D ± L, 4.6 ± 250 mm; No. 238EV54) where H_2O with 0.1% TFA (v/v) constituted the stationary phase (solvent A) and 95% acetonitrile, 0.1% TFA (v/v) the mobile phase (solvent B) (Figure S1D). We first reconstituted the venom in 5% solvent B then separated its constituents with a linear gradient (0.8 ml min^{-1}) of 5–40% solvent B. We collected the resultant fractions, evaporated organic solvent under vacuum, and flash froze them in LN_2. We next lyophilized, sealed, and stored fractions at −80 ° C until use. Of fractionated venom components, a single fraction recapitulated the crude venom's TRPA1-activating activity (Figure S1F). We mixed this fraction1:1 (v/v) with 5 mg ml^{-1} α-cyano-4-hydroxycinnamic acid (CHCA) matrix before spotting the solution onto a target for mass spectrometry (MS) analysis. We collected externally calibrated (ProteoMass Kit, MilliporeSigma) spectra over a range of 1000–5000 *m/z* on an Axima Performace MALDI-ToF/ToF mass spectrometer (Shimadzu) in reflectron mode. These spectra displayed a single species of $[M+H]^+$ 3854.5 (Figure S1E).

To determine this peptide's sequence *de novo*, we purified ~50 pmol from 5 mg venom as above, then reduced and alkylated the resulting material with 500-fold molar excess TCEP at 37 ° C for 30 min. followed by 500-fold molar excess Iodoacetamide (IAM) at RT for 30 min. in 25 mM NH_4HCO_3. We then analyzed linear, partially cysteine carbamidomethylated (C^{AM}) toxin via nanospray sample introduction into an LTQ-Orbitrap Velos tandem mass spectrometer (Thermo Scientific). We acquired ion trap collision-induced dissociation (CID) and beam-type higher-energy C-trap dissociation (HCD) spectra from *m/z* 1007.9475 (4^+), which represents the toxin featuring three C^{AM}. We then measured fragments from both activation methods were measure with high resolution in the Orbitrap. Manual interpretation of the resulting CID and HCD spectra yielded a complete mature peptide sequence (Figure S1G; Table S1) of calculated oxidized $[M+H]^+$ 3853.7, in reasonable agreement with our MALDI-ToF analysis. We confirmed the identity the WaTx's N-terminal dipeptide by carrying out a tBLASTn search against an extant *U. manicatus* venom gland transcriptome (SRX288428) (Sunagar et al., 2013), which also yielded candidate signal and pro-peptide sequences (Figure S1g). We inferred WaTx's disulfide bonding pattern based on homology considerations with κ-KTx family of peptide toxins (Figure 1C) (Srinivasan et al., 2002). Based on this phylogeny, WaTx may also be referred to as κ-KTx 6.1 (Tytgat et al., 1999) and/or τ-Scorpionitoxin-Um1a (King et al., 2008).

We purchased synthetic WaTx and WaTx mutants from AnaSpec (Fremont, CA) or LifeTein (Somerset, NJ). These companies produced mature, folded, and by chemical synthesis with directed disulfide bond formation between C9-C27 and C13-C23 at 5 mg scale to > 90% purity, as assessed by HPLC. Because of the low abundance of (~10 pmol mg^{-1} venom) of toxin in venom and limited availability of scorpions for milking, we used synthetic WaTx in all further experiments. For all assays, we resuspended and aliquoted synthetic WaTx in H_2O upon delivery. We immediately flash froze these aliquots in LN_2; then lyophilized, sealed, and stored them at −80 ° C until use. We confirmed the proper folding of WaTx and mutants using CD spectroscopy; these data were collected over a 1 mm pathlength across 190–250 nm on an Aviv CD Spectrometer 215 using 10 μM WaTx in PBS, pH 7.4, then processed in CDToolX (Miles and Wallace, 2018).

Author Manuscript Author Manuscript Author Manuscript Author Manuscript

Ca^{2+} imaging—Prior to imaging, we loaded adhered cells with indicator solution (Ringer's solution containing 0.1 mg ml^{-1} Fura-2 AM dye and 0.02% (w/v) Pluronic F-127 for 30 min. at room temperature (RT) in the dark. We then excited cells using either a Lamda LS (Sutter) (Figure 1B; S1C, F, and K; S3A) or DG-4 illuminator (Sutter) (Figure 1A; S1H–K; S3F, H). We collected fluorescent emissions with an ORCA-ER camera and controller (Hamamatsu), and digitized and analyzed the data with MetaFluor (Molecular Devices). To quantify the data, we calculated the ratio of 340 to 380 nm fluorescence after background subtraction. Experiments were carried out either with cells adhered to a glass slide coated with poly-L and isolated in silicon wells (O.D. x Depth, 2.5 × 2.0 mm) Figure 1B; S1C, F, and K; S3A); or to a coverslip coated with poly-L (HEK) or PLL (neurons) in order to make pharmacological manipulations under laminar flow using a pressure-driven micro-perfusion system (SmartSquirt, Automate Scientific) (Figure 1A; S1H–K; S3F, H).

Electrophysiology—We fashioned capillary glass pipettes from borosilicate glass with filament (O.D ± I.D, 1.10 ± 0.86 mm, Sutter Instruments) and fire-polished them a resistance of 2–5m for whole-cell or 6–12mΩ for excised-patch patch-clamp recordings. We then made electrophysiological measurements at RT using an Axopatch 200B amplifier (Axon Instruments) and digitized the data with a Digidata 1550B (Axon Instruments). We executed voltage protocols and monitored resulting currents on-line with pClamp10 (Molecular Devices), which we analyzed off-line in pClamp and Prism (GraphPad). We carried out all electrophysiological recordings and pharmacological manipulations under laminar flow using a pressure-driven micro-perfusion system (SmartSquirt, Automate Scientific).

We performed whole-cell recordings in a bath solution of nominally Ca^{2+}-free Ringer's solution, sampling data at 10 kHz and filtering it at 1 kHz. For TRP channels, we used an internal solution containing, in mM, 140 $CsMeSO_4$, 10 HEPES, 1 $MgCl_2$, and 1 EGTA; pH 7.2 with CsOH; 300–310 mOsm kg^{-1} with sucrose. For K_v channels, we replaced $CsMeSO_4$ with equimolar $KMeSO_4$, pH 7.2 with KOH in the pipette. Unless otherwise stated, I-V curves were generated from whole-cell patch clamp recordings in response to 500 msec. steps from −80 to 80 mV in 10 mV increments. Tail-current measurements (Figure 1C, and S4A, B) were made at −120 mV following 500 ms steps from −80 to 80 mV in 10mV increments or 70 to 145mV in 15mV increments in whole-cell patch-clamp mode. Data were leak-subtracted on-line (P/4), normalized to the currents obtained at 70 mV, then fit by non-linear regression to the Boltzmann equation to determine $V_{1/2}$.

We carried out cell-attached and excised-patch recordings in symmetrical solutions of, in mM, 150 NaCl, 10 HEPES, 2 EGTA, 1 $MgCl_2$, 1 IP_6, 6 NaOH; pH 7.3 with NaOH; 300–310 mOsm kg^{-1}; sampling at 20 KHz and filtering at 2 kHz. For monovalent cation selectivity experiments (Figure 4F; S5D, E), the bath solution contained in mM, 150 NaCl, 10 HEPES, 2 EGTA, 1 IP_6, 6 NaOH at pH 7.3 with NaOH and 300–310 mOsm kg^{-1}. The pipette solution was identical except we replaced Na^+ with equimolar K^+, Cs^+, Li^+, or $NMDG^+$ and set to pH 7.3 with, as appropriate, KOH, CsOH, or Trizma. For divalent cation selectivity experiments, the bath solution contained, in mM: 75 $CaCl_2$ or $MgCl_2$, 10 HEPES, pH 7.3 with Trizma; 300–310 mOsm kg^{-1}. The pipette solution contained in mM: 150 NaCl, 10 HEPES, 2 EGTA, 1 IP_6, 6 NaOH; pH 7.3 with NaOH; 300–310 mOsm kg^{-1}. We determined the reversal potential as the minimum of the standard deviation of the average

Author Manuscript Author Manuscript Author Manuscript Author Manuscript

trace resultant from at least 10 sweeps of a 500 ms. ramp from −100 to 80 mV under a given pharmacological condition (Bobkov et al., 2011) (Figure S4F, G). We then calculated relative permeability ratios using this value to solve the Goldman-Hodgkin-Katz equation (Hille, 2001).

FRET-based liposome loading—After drying soybean polar lipids (Avanti) under argon and dessicating them for 1 hr. under vacuum, we resuspended lipids in liposome buffer containing (in mM) 150 NaCl and 10 HEPES pH 7.4 followed by bath sonication for 10 min. We doped fluorophore AlexaFluor568-IgG (donkey anti-goat, Thermo-Fisher, No A11057.) was to this mixture to a final concentration of 2 μg ml^{-1}. We next fashioned large unilamellar vesicles (LUVs, ~100 nm mean diameter) by extrusion through a 0.2 μm filter. To remove unincorporated acceptor fluorophore, we pelleted LUVs at 100,000 x *g* for 40 min. at 4° C. We then resuspended liposomes in liposome buffer to a concentration of 2 mg ml^{-1} with 1000-fold molar excess Trypan Blue dye to quench extra-liposomal excitatory fluorescence. We serially diluted N-terminal conjugated green fluorescent WaTx (AlexaFluor488-K-WaTx or WaTx K7A, LifeTein) into 96-well plates containing liposomes for Förester resonance energy transfer (F RET) analysis. We then collected FRET emission every min. for 30 min. at 23 ° C using an excitation wavelength of 480 nm and emission wavelength of 570 nm on a Synergy H4 plate reader (BioTek). After subtracting background excitation fluorescence from donor and acceptor fluorophore-only conditions, we fit the data fitting with a one-phase association exponential function in Prism to derive the FRET curves and kinetic parameters of loading shown (Figure 2D, E).

WaTx structure determination—We suspended WaTx at 300 μM in 0.38 mm thin walled glass tubes rated 600 MHz (O.D. ± Length, 5 ± 1778 mm; Wilmad LabGlass, No. 535-PP-7) in unbuffered 10 or 100 % (v/v) D_2O, pH < 4.0. We collected [^{1}H, ^{1}H]-COSY, TOCSY, and NOESY spectra, and natural abundance [^{13}C, ^{1}H]-HSQC spectra at ambient temperature on an 800 MHz NMR spectrometer (Bruker Avance I 800) using a Z-gradient 5mm TXI Cryoprobe at 298 K, then processed the data in TopSpin (Bruker). We referenced proton chemical shifts to an external DSS standard and ^{13}C shifts indirectly from this value. We then manually assigned resonances and generated restraints in CCPN Analysis (Vranken et al., 2005) (Figure S3J, K; Table S2). DANGLE (Cheung et al., 2010) predicted additional dihedral restraints from the NOESY and HSQC assignments. We calculated structures with ARIA (Rieping et al., 2007) and evaluated their quality with PSVS (Bhattacharya et al., 2007). In the final iteration, we solved 200 structures then refined 50, selected based on total energy, in explicit water (Table S2). We deposited these models (All-atom RMSD = 0.332) and underlying NMR data to the PDB and BMRB with accession codes 6OFA and 30597, respectively.

Biolayer Interferometry—We transfected HEK cells for 14 hrs. in DMEM-C with 3 μg of indicated constructs mixed with 3x (w/w) Lipofectamine 2000 (Thermo-Fisher). We washed cells once with PBS, then harvested them with buffer containing (in mM) 320 sucrose, 50 tris-Cl pH 7.5, 1 EDTA, 1 IP_6, 6 NaOH, and 1x Protease Inhibitor Cocktail (Roche). After isolating live cells floated by centrifugation at 750 x *g* for 10 min at 4° C we pelleted them by centrifugation at 100,000 x *g* for 45 min at 4° C. We mechanically homogenized this

Author Manuscript Author Manuscript Author Manuscript Author Manuscript

pellet in harvest buffer (minus sucrose) to generate crude membranes (Maricq et al., 1991), then diluted these fragments to 0.5 mg ml^{-1} protein content as determined by Bradford assay (Bradford, 1976). We used 100–1000 μg crude membranes for analysis by biolayer interferometry on an OctetRed 394 instrument (Pall/ForteBio) using N-terminal biotinylated toxin (Biotin-GSGS-WaTx, LifeTein) coupled to streptavidin sensors (Pall/ForteBio) as a probe. Sensorgrams from mock-transfected membranes measured non-specific binding, which we then subtracted on-line. We determined the kinetic parameters for WaTx:hTRPA1 binding directly (k_{off}) or by estimation (k_{on} and K_D) assuming a concentration of 1 pM TRPA1 binding sites. We made this estimate by controlling the total live cell input to the assay (~2.0 ± 10^6) and assuming a lowest-affinity binding scenario where (1) WaTx binds 1:1 to TRPA1 monomers and (2) each cell expresses the maximum number of TRPA1 channels—approximately 1000, equivalent to 4000 receptor sites. This second assumption was made based on our electrophysiological studies of receptor, *cf.* Figure 1D D; S4I).

Animal Behavior—For all experiments, treatment consisted of 20 μL 0.9% (w/v) saline (vehicle), WaTx dissolved in vehicle, or 0.75% (v/v) AITC in mineral oil injected intraplantar to the hindpaw. After treatment, we scored nocifensive behavior (biting and/or licking of the injected paw) for 20 min. immediately following injection. We quantified thermal hypersensitivity as the latency to first nocifensive response (flinch, bite, and/or lick) of the injected paw on a 48 ° C hotplate, and mechanical allodynia by applying von Frey hairs (0.008 – 4.0 g) applied to the treated paw and scoring the responses using the Up-Down method (Chaplan et al., 1994). To assess neurogenic inflammation, we quantified local edema as an increase in paw thickness, measured by digital calipers (VWR), and as an increase vascular permeability, measured by Evan's Blue Dye (EBD) extravasation at one hr. post-algesic injection. We injected EBD (0.5% (w/v) in PBS) retro-orbitally (20 mg kg^{-1}) prior to the experiment; following caliper measurements we euthanized the mice and extracted EBD from the paw as described previously (Zhang et al., 2017), then quantified EBD extravasation via 620 nm absorption on a spectrophotometer. Finally, we carried out intrathecal capsaicin ablations as described previously (Cavanaugh et al., 2009; Emrick et al., 2018; Osteen et al., 2016), and confirmed ablation by hotplate test at 50 ° C (Figure S6E). We collected and scored all behavioral data such that the experimenter was blind to either the mouse genotype, treatment received, or both.

Immunohistochemistry—We anesthetized adult mice with pentobarbital then perfused them transcardially with PBS followed by 10% neutral buffered formalin (NBF). We dissected, postfixed in 10% NBF at 4 °C overnight (O/N), then cryoprotected spinal cords in PBS with 30% (w/v) sucrose O/N at 4 °C. Before sectioning, we embedded tissue samples in OCT compound (VWR) at −20 °C. We then thaw-captured 20 μm spinal cord sections prepared from segments L4/L5 with a Leica CM3050 S cryostat onto glass slides. We blocked slides containing sections of spinal cord for 1 hr. at RT in PBS plus 0.1% (v/v) Triton X-100 (PBST) with 10% normal goat serum (NGS). Then we rinsed slides once with PBST containing 2.5% NGS and incubated them O/N with rabbit anti-Fos (1:2,000; Biosensis, No. R-1751–25) in PBST with 2.5% NGS at 4 °C. Following incubation, we washed slides thrice in PBS, rinsed once with PBST, then incubated them in secondary antibody (1:1,000; goat anti-rabbit AlexaFluor488-IgG, Thermo-Fisher, No. A11034) for 2

Author Manuscript Author Manuscript Author Manuscript Author Manuscript

hrs. in PBST at RT in the dark. Following incubation, we washed slides thrice with PBS then mounted them in ProLong Gold antifade reagent with DAPI (Thermo-Fisher) under a coverslip. We acquired epifluorescent images with a Leica DMRB microscope mounted with an Infinity 3–3UR Monochrome CCD digital camera using Infinity Analyze software. Following capture, we analyzed and false-colored (grayscale) micrographs in ImageJ. We counted cFos-positive cells blind to genotype and treatment.

Enzyme-linked Immunosorbent Assay (ELISA)—Enzyme-linked immunosorbent assays detected CGRP release from 1 DIV primary rat trigeminal neurons (harvested on P0-P1), cultured as described above. To prepare cultures, we applied either indicated treatments (Figure 5i) for 5 min. at RT. We pooled supernatants from three replicate coverslips into a single well of a 96-well plate containing a monoclonal anti-human CGRP antibody (rat cross-reactivity: 120%; Bertin Bioreagents, No. A08481) and incubated them overnight at 4 ° C, then developed them per the manufacturer's instructions (Bertin Bioreagents, No. A05481). Briefly, we first added acetylcholinesterase coupled to an anti-CGRP antibody (No. A04481), then monitored cleavage of dithio-bis-nitrobenzoic acid (DTNB) via increased TNB fluorescence at 414nm on a Synergy H4 plate reader (BioTek) every min. for 30 min. We determined the amount (pg ml^{-1}) of CGRP release (by comparison to a standard curve derived from purified CGRP (Bertin Bioreagents, No. A05481), and normalized all data to the amount of CGRP released by AITC treatment.

QUANTIFICATION AND STATISTICAL ANALYSIS

Herein we summarized data using the mean ± SEM unless otherwise noted. We carried out statistical testing in Prism (GraphPad) using either a two-tailed student's *t* test, or One- or Two-Way ANOVA with a *post-hoc* Holm-Sidak correction for multiple comparisons, as indicated in the figure legends. *A priori*, we set $\alpha = 0.05$ and represent statistical significance as: * $P < 0.05$, ** $P < 0.01$, *** $P < 0.001$, and **** $P < 0.0001$. Parametric significance tests assuming equal variance and a normal distribution of data means are justified given the experimental design, and are the standard tests for similar experiments. We selected sample sizes for all experiments on the basis of our laboratory and others' experience with similar assays, and in consideration of reagent availability and technical feasibility. We made no predetermination of sample size and thus carried out a minimum of independent experiments required for statistical significance and reproducibility.

DATA AVAILABILITY

The WaTx peptide sequence has been deposited to UniProt with accession code C0HLG4. Atomic coordinates for the solution structural ensemble of WaTx and underlying NMR chemical shifts and peaks have been deposited to the PDB and BMRB with accession codes 6OFA and 30597, respectively.

Supplementary Material

Refer to Web version on PubMed Central for supplementary material.

Author Manuscript Author Manuscript Author Manuscript Author Manuscript

Acknowledgements

We thank all members of the Julius lab for provocative discussions, especially N. Bellono for guidance and advice with patch-clamp electrophysiology and D. Leitch for guidance with interpretation of transcriptomic data. We also recognize J. Poblete and J. Braz for expert technical assistance with mouse experiments. Finally, we are grateful to L.Y. Jan, R.A. Nicoll, D. Cohn, and W.J. Tang for their critical reading of the manuscript. This work was supported by an NSF Graduate Research Fellowship (No. 1650113 to J.V.L.K), a UCSF Chuan-Lyu Discovery Fellowship (J.V.L.K), and grants from the NIH (R37 NS065071 and R35 NS105038 to D.J; and T32 GM007449 to J.V.L.K).

References

Andersson DA, Gentry C, Moss S, and Bevan S (2008). Transient receptor potential A1 is a sensory receptor for multiple products of oxidative stress. The Journal of neuroscience : the official journal of the Society for Neuroscience 28, 2485–2494. [PubMed: 18322093]

Bahia PK, Parks TA, Stanford KR, Mitchell DA, Varma S, Stevens SM Jr., and Taylor-Clark TE (2016). The exceptionally high reactivity of Cys 621 is critical for electrophilic activation of the sensory nerve ion channel TRPA1. The Journal of general physiology 147, 451–465. [PubMed: 27241698]

Baker NA, Sept D, Joseph S, Holst MJ, and McCammon JA (2001). Electrostatics of nanosystems: application to microtubules and the ribosome. Proceedings of the National Academy of Sciences of the United States of America 98, 10037–10041. [PubMed: 11517324]

Bandell M, Story GM, Hwang SW, Viswanath V, Eid SR, Petrus MJ, Earley TJ, and Patapoutian A (2004). Noxious cold ion channel TRPA1 is activated by pungent compounds and bradykinin. Neuron 41, 849–857. [PubMed: 15046718]

Banzawa N, Saito S, Imagawa T, Kashio M, Takahashi K, Tominaga M, and Ohta T (2014). Molecular Basis Determining Inhibition/Activation of Nociceptive Receptor TRPA1 Protein: A Single Amino Acid Dictates Species-specific actions of the most potent mammalian TRPA1 Antagonist. Journal of Biological Chemistry 289, 31927–31939. [PubMed: 25271161]

Basbaum AI, Bautista DM, Scherrer G, and Julius D (2009). Cellular and molecular mechanisms of pain. Cell 139, 267–284. [PubMed: 19837031]

Bautista DM, Jordt SE, Nikai T, Tsuruda PR, Read AJ, Poblete J, Yamoah EN, Basbaum AI, and Julius D (2006). TRPA1 mediates the inflammatory actions of environmental irritants and proalgesic agents. Cell 124, 1269–1282. [PubMed: 16564016]

Bautista DM, Pellegrino M, and Tsunozaki M (2013). TRPA1: A gatekeeper for inflammation. Annual review of physiology 75, 181–200.

Bechara C, and Sagan S (2013). Cell-penetrating peptides: 20 years later, where do we stand? FEBS letters 587, 1693–1702. [PubMed: 23669356]

Bhattacharya A, Tejero R, and Montelione GT (2007). Evaluating protein structures determined by structural genomics consortia. Proteins 66, 778–795. [PubMed: 17186527]

Bobkov YV, Corey EA, and Ache BW (2011). The pore properties of human nociceptor channel TRPA1 evaluated in single channel recordings. Biochimica et biophysica acta 1808, 1120–1128. [PubMed: 21195050]

Bohlen CJ, Chesler AT, Sharif-Naeini R, Medzihradszky KF, Zhou S, King D, Sanchez EE, Burlingame AL, Basbaum AI, and Julius D (2011). A heteromeric Texas coral snake toxin targets acid-sensing ion channels to produce pain. Nature 479, 410–414. [PubMed: 22094702]

Bohlen CJ, and Julius D (2012). Receptor-targeting mechanisms of pain-causing toxins: How ow? Toxicon : official journal of the International Society on Toxinology 60, 254–264. [PubMed: 22538196]

Bohlen CJ, Priel A, Zhou S, King D, Siemens J, and Julius D (2010). A bivalent tarantula toxin activates the capsaicin receptor, TRPV1, by targeting the outer pore domain. Cell 141, 834–845. [PubMed: 20510930]

Bosmans F, and Tytgat J (2007). Voltage-gated sodium channel modulation by scorpion alpha-toxins. Toxicon : official journal of the International Society on Toxinology 49, 142–158. [PubMed: 17087986]

Author Manuscript Author Manuscript Author Manuscript Author Manuscript

Bradford MM (1976). A rapid and sensitive method for the quantitation of microgram quantities of protein utilizing the principle of protein-dye binding. Analytical biochemistry 72, 248–254. [PubMed: 942051]

Cao E, Liao M, Cheng Y, and Julius D (2013). TRPV1 structures in distinct conformations reveal activation mechanisms. Nature 504, 113–118. [PubMed: 24305161]

Caterina MJ, Leffler A, Malmberg AB, Martin WJ, Trafton J, Petersen-Zeitz KR, Koltzenburg M, Basbaum AI, and Julius D (2000). Impaired Nociception and Pain Sensation in Mice Lacking the Capsaicin Receptor. Science 288, 306. [PubMed: 10764638]

Caterina MJ, Schumacher MA, Tominaga M, Rosen TA, Levine JD, and Julius D (1997). The capsaicin receptor: a heat-activated ion channel in the pain pathway. Nature 389, 816–824. [PubMed: 9349813]

Cavanaugh DJ, Lee H, Lo L, Shields SD, Zylka MJ, Basbaum AI, and Anderson DJ (2009). Distinct subsets of unmyelinated primary sensory fibers mediate behavioral responses to noxious thermal and mechanical stimuli. Proceedings of the National Academy of Sciences of the United States of America 106, 9075–9080. [PubMed: 19451647]

Chaplan SR, Bach FW, Pogrel JW, Chung JM, and Yaksh TL (1994). Quantitative assessment of tactile allodynia in the rat paw. Journal of Neuroscience Methods 53, 55–63. [PubMed: 7990513]

Chen J, Joshi SK, DiDomenico S, Perner RJ, Mikusa JP, Gauvin DM, Segreti JA, Han P, Zhang XF, Niforatos W, et al. (2011). Selective blockade of TRPA1 channel attenuates pathological pain without altering noxious cold sensation or body temperature regulation. Pain 152, 1165–1172. [PubMed: 21402443]

Cheung MS, Maguire ML, Stevens TJ, and Broadhurst RW (2010). DANGLE: A Bayesian inferential method for predicting protein backbone dihedral angles and secondary structure. Journal of magnetic resonance 202, 223–233. [PubMed: 20015671]

Chung MK, Guler AD, and Caterina MJ (2008). TRPV1 shows dynamic ionic selectivity during agonist stimulation. Nature neuroscience 11, 555–564. [PubMed: 18391945]

Clapham DE (2003). TRP channels as cellular sensors. Nature 426, 517–524. [PubMed: 14654832]

Cordero-Morales JF, Gracheva EO, and Julius D (2011). Cytoplasmic ankyrin repeats of transient receptor potential A1 (TRPA1) dictate sensitivity to thermal and chemical stimuli. Proceedings of the National Academy of Sciences of the United States of America 108, E1184–E1191. [PubMed: 21930928]

Derossi D, Joliot AH, Chassaing G, and Prochiantz A (1994). The third helix of the Antennapedia homeodomain translocates through biological membranes. The Journal of biological chemistry 269, 10444–10450. [PubMed: 8144628]

Emrick JJ, Mathur A, Wei J, Gracheva EO, Gronert K, Rosenblum MD, and Julius D (2018). Tissue-specific contributions of *Tmem79* to atopic dermatitis and mast cell-mediated histaminergic itch. Proceedings of the National Academy of Sciences 115, E12091.

Felder CE, Prilusky J, Silman I, and Sussman JL (2007). A server and database for dipole moments of proteins. Nucleic acids research 35, W512–W521. [PubMed: 17526523]

Frankel AD, and Pabo CO (1988). Cellular uptake of the tat protein from human immunodeficiency virus. Cell 55, 1189–1193. [PubMed: 2849510]

Gao Y, Cao E, Julius D, and Cheng Y (2016). TRPV1 structures in nanodiscs reveal mechanisms of ligand and lipid action. Nature 534, 347–351. [PubMed: 27281200]

Gracheva EO, Cordero-Morales JF, González-Carcacía JA, Ingolia NT, Manno C, Aranguren CI, Weissman JS, and Julius D (2011). Ganglion-specific splicing of TRPV1 underlies infrared sensation in vampire bats. Nature 476, 88. [PubMed: 21814281]

Gracheva EO, Ingolia NT, Kelly YM, Cordero-Morales JF, Hollopeter G, Chesler AT, Sanchez EE, Perez JC, Weissman JS, and Julius D (2010). Molecular basis of infrared detection by snakes. Nature 464, 1006–1011. [PubMed: 20228791]

Guidotti G, Brambilla L, and Rossi D (2017). Cell-Penetrating Peptides: From Basic Research to Clinics. Trends in Pharmacological Sciences 38, 406–424. [PubMed: 28209404]

Heitz F, Morris MC, and Divita G (2009). Twenty years of cell-penetrating peptides: from molecular mechanisms to therapeutics. Br J Pharmacol 157, 195–206. [PubMed: 19309362]

Hille B (2001). Ion channels of excitable membranes (Sinauer).

Author Manuscript Author Manuscript Author Manuscript Author Manuscript

Hinman A, Chuang HH, Bautista DM, and Julius D (2006). TRP channel activation by reversible covalent modification. Proceedings of the National Academy of Sciences of the United States of America 103, 19564–19568. [PubMed: 17164327]

Horn R (1991). Diffusion of nystatin in plasma membrane is inhibited by a glass-membrane seal. Biophysical journal 60, 329–333. [PubMed: 1912275]

Joliot A, Pernelle C, Deagostini-Bazin H, and Prochiantz A (1991). Antennapedia homeobox peptide regulates neural morphogenesis. Proceedings of the National Academy of Sciences of the United States of America 88, 1864–1868. [PubMed: 1672046]

Joliot A, and Prochiantz A (2004). Transduction peptides: from technology to physiology. Nat Cell Biol 6, 189–196. [PubMed: 15039791]

Jordt SE, Bautista DM, Chuang HH, McKemy DD, Zygmunt PM, Hogestatt ED, Meng ID, and Julius D (2004). Mustard oils and cannabinoids excite sensory nerve fibres through the TRP channel ANKTM1. Nature 427, 260–265. [PubMed: 14712238]

Julius D (2013). TRP channels and pain. Annual review of cell and developmental biology 29, 355–384.

Jung HJ, Lee JY, Kim SH, Eu Y-J, Shin SY, Milescu M, Swartz KJ, and Kim JI (2005). Solution Structure and Lipid Membrane Partitioning of VSTx1, an Inhibitor of the KvAP Potassium Channel. Biochemistry 44, 6015–6023. [PubMed: 15835890]

Kalia J, Milescu M, Salvatierra J, Wagner J, Klint JK, King GF, Olivera BM, and Bosmans F (2015). From foe to friend: using animal toxins to investigate ion channel function. Journal of molecular biology 427, 158–175. [PubMed: 25088688]

Kang K, Pulver SR, Panzano VC, Chang EC, Griffith LC, Theobald DL, and Garrity PA (2010). Analysis of Drosophila TRPA1 reveals an ancient origin for human chemical nociception. Nature 464, 597–600. [PubMed: 20237474]

Karashima Y, Damann N, Prenen J, Talavera K, Segal A, Voets T, and Nilius B (2007). Bimodal Action of Menthol on the Transient Receptor Potential Channel TRPA1. The Journal of Neuroscience 27, 9874. [PubMed: 17855602]

Karashima Y, Prenen J, Talavera K, Janssens A, Voets T, and Nilius B (2010). Agonist-induced changes in Ca(2+) permeation through the nociceptor cation channel TRPA1. Biophysical journal 98, 773–783. [PubMed: 20197030]

Kauffman WB, Fuselier T, He J, and Wimley WC (2015). Mechanism Matters: A Taxonomy of Cell Penetrating Peptides. Trends in biochemical sciences 40, 749–764. [PubMed: 26545486]

Kindt KS, Viswanath V, Macpherson L, Quast K, Hu H, Patapoutian A, and Schafer WR (2007). Caenorhabditis elegans TRPA-1 functions in mechanosensation. Nature neuroscience 10, 568–577. [PubMed: 17450139]

King GF, Gentz MC, Escoubas P, and Nicholson GM (2008). A rational nomenclature for naming peptide toxins from spiders and other venomous animals. Toxicon : official journal of the International Society on Toxinology 52, 264–276. [PubMed: 18619481]

King GF, and Hardy MC (2013). Spider-venom peptides: structure, pharmacology, and potential for control of insect pests. Annual review of entomology 58, 475–496.

Latorre R, Zaelzer C, and Brauchi S (2009). Structure-functional intimacies of transient receptor potential channels. Quarterly reviews of biophysics 42, 201–246. [PubMed: 20025796]

Lee SY, and MacKinnon R (2004). A membrane-access mechanism of ion channel inhibition by voltage sensor toxins from spider venom. Nature 430, 232–235. [PubMed: 15241419]

Liao M, Cao E, Julius D, and Cheng Y (2013). Structure of the TRPV1 ion channel determined by electron cryo-microscopy. Nature 504, 107–112. [PubMed: 24305160]

Lipscombe D, Kongsamut S, and Tsien RW (1989). Alpha-adrenergic inhibition of sympathetic neurotransmitter release mediated by modulation of N-type calcium-channel gating. Nature 340, 639–642. [PubMed: 2570354]

Macpherson LJ, Dubin AE, Evans MJ, Marr F, Schultz PG, Cravatt BF, and Patapoutian A (2007). Noxious compounds activate TRPA1 ion channels through covalent modification of cysteines. Nature 445, 541–545. [PubMed: 17237762]

Author Manuscript Author Manuscript Author Manuscript Author Manuscript

Maricq AV, Peterson AS, Brake AJ, Myers RM, and Julius D (1991). Primary structure and functional expression of the 5HT3 receptor, a serotonin-gated ion channel. Science 254, 432–437. [PubMed: 1718042]

McKemy DD, Neuhausser WM, and Julius D (2002). Identification of a cold receptor reveals a general role for TRP channels in thermosensation. Nature 416, 52–58. [PubMed: 11882888]

McNamara CR, Mandel-Brehm J, Bautista DM, Siemens J, Deranian KL, Zhao M, Hayward NJ, Chong JA, Julius D, Moran MM, et al. (2007). TRPA1 mediates formalin-induced pain. Proceedings of the National Academy of Sciences of the United States of America 104, 13525–13530. [PubMed: 17686976]

Mihailescu M, Krepkiy D, Milescu M, Gawrisch K, Swartz KJ, and White S (2014). Structural interactions of a voltage sensor toxin with lipid membranes. Proceedings of the National Academy of Sciences 111, E5463.

Miles AJ, and Wallace BA (2018). CDtoolX, a downloadable software package for processing and analyses of circular dichroism spectroscopic data. Protein Science 27, 1717–1722. [PubMed: 30168221]

Moran MM (2018). TRP Channels as Potential Drug Targets. Annual Review of Pharmacology and Toxicology 58, 309–330.

Nagata K, Duggan A, Kumar G, and Garcia-Anoveros J (2005). Nociceptor and hair cell transducer properties of TRPA1, a channel for pain and hearing. J Neurosci 25, 4052–4061. [PubMed: 15843607]

Nicoll RA, Eccles JC, Oshima T, and Rubia F (1975). Prolongation of hippocampal inhibitory postsynaptic potentials by barbiturates. Nature 258, 625. [PubMed: 1207741]

Nilius B, Prenen J, and Owsianik G (2011). Irritating channels: the case of TRPA1. The Journal of physiology 589, 1543–1549. [PubMed: 21078588]

Osteen JD, Herzig V, Gilchrist J, Emrick JJ, Zhang C, Wang X, Castro J, Garcia-Caraballo S, Grundy L, Rychkov GY, et al. (2016). Selective spider toxins reveal a role for the Nav1.1 channel in mechanical pain. Nature 534, 494–499. [PubMed: 27281198]

Palovcak E, Delemotte L, Klein ML, and Carnevale V (2015). Comparative sequence analysis suggests a conserved gating mechanism for TRP channels. The Journal of general physiology 146, 37–50. [PubMed: 26078053]

Paulsen CE, Armache JP, Gao Y, Cheng Y, and Julius D (2015). Structure of the TRPA1 ion channel suggests regulatory mechanisms. Nature 520, 511–517. [PubMed: 25855297]

Peier AM, Moqrich A, Hergarden AC, Reeve AJ, Andersson DA, Story GM, Earley TJ, Dragoni I, McIntyre P, Bevan S, et al. (2002). A TRP channel that senses cold stimuli and menthol. Cell 108, 705–715. [PubMed: 11893340]

Prober DA, Zimmerman S, Myers BR, McDermott BM, Kim S-H, Caron S, Rihel J, Solnica-Krezel L, Julius D, Hudspeth AJ, et al. (2008). Zebrafish TRPA1 Channels Are Required for Chemosensation But Not for Thermosensation or Mechanosensory Hair Cell Function. The Journal of Neuroscience 28, 10102. [PubMed: 18829968]

Quintero-Hernandez V, Jimenez-Vargas JM, Gurrola GB, Valdivia HH, and Possani LD (2013). Scorpion venom components that affect ion-channels function. Toxicon : official journal of the International Society on Toxinology 76, 328–342. [PubMed: 23891887]

Rieping W, Habeck M, Bardiaux B, Bernard A, Malliavin TE, and Nilges M (2007). ARIA2: automated NOE assignment and data integration in NMR structure calculation. Bioinformatics (Oxford, England) 23, 381–382.

Sakmann B, and Neher E (2009). Single-channel recording (Springer).

Shi G, Kleinklaus AK, Marrion NV, and Trimmer JS (1994). Properties of Kv2.1 K+ channels expressed in transfected mammalian cells. The Journal of biological chemistry 269, 23204–23211. [PubMed: 8083226]

Siemens J, Zhou S, Piskorowski R, Nikai T, Lumpkin EA, Basbaum AI, King D, and Julius D (2006). Spider toxins activate the capsaicin receptor to produce inflammatory pain. Nature 444, 208–212. [PubMed: 17093448]

Silva PI Jr., Daffre S, and Bulet P (2000). Isolation and characterization of gomesin, an 18-residue cysteine-rich defense peptide from the spider Acanthoscurria gomesiana hemocytes with sequence

Author Manuscript Author Manuscript Author Manuscript Author Manuscript

similarities to horseshoe crab antimicrobial peptides of the tachyplesin family. The Journal of biological chemistry 275, 33464–33470. [PubMed: 10942757]

Srinivasan KN, Sivaraja V, Huys I, Sasaki T, Cheng B, Kumar TK, Sato K, Tytgat J, Yu C, San BC, et al. (2002). kappa-Hefutoxin1, a novel toxin from the scorpion Heterometrus fulvipes with unique structure and function. Importance of the functional diad in potassium channel selectivity. The Journal of biological chemistry 277, 30040–30047. [PubMed: 12034709]

Story GM, Peier AM, Reeve AJ, Eid SR, Mosbacher J, Hricik TR, Earley TJ, Hergarden AC, Andersson DA, Hwang SW, et al. (2003). ANKTM1, a TRP-like Channel Expressed in Nociceptive Neurons, Is Activated by Cold Temperatures. Cell 112, 819–829. [PubMed: 12654248]

Sunagar K, Undheim EAB, Chan AHC, Koludarov I, Muñoz-Gómez SA, Antunes A, and Fry BG (2013). Evolution stings: the origin and diversification of scorpion toxin peptide scaffolds. Toxins 5, 2456–2487. [PubMed: 24351712]

Thorell T (1876). On the classification of scorpions. The annals and magazine of natural history; zoology, botany, and geology 4, 1–15.

Tominaga M, Caterina MJ, Malmberg AB, Rosen TA, Gilbert H, Skinner K, Raumann BE, Basbaum AI, and Julius D (1998). The cloned capsaicin receptor integrates multiple pain-producing stimuli. Neuron 21, 531–543. [PubMed: 9768840]

Twyman RE, Rogers CJ, and Macdonald RL (1989). Differential regulation of γ-aminobutyric acid receptor channels by diazepam and phenobarbital. Annals of Neurology 25, 213–220. [PubMed: 2471436]

Tytgat J, Chandy KG, Garcia ML, Gutman GA, Martin-Eauclaire M-F, van der Walt JJ, and Possani LD (1999). A unified nomenclature for short-chain peptides isolated from scorpion venoms: α-KTx molecular subfamilies. Trends in Pharmacological Sciences 20, 444–447. [PubMed: 10542442]

Venkatachalam K, and Montell C (2007). TRP Channels. Annual Review of Biochemistry 76, 387–417.

Vives E, Brodin P, and Lebleu B (1997). A truncated HIV-1 Tat protein basic domain rapidly translocates through the plasma membrane and accumulates in the cell nucleus. The Journal of biological chemistry 272, 16010–16017. [PubMed: 9188504]

Vranken WF, Boucher W, Stevens TJ, Fogh RH, Pajon A, Llinas M, Ulrich EL, Markley JL, Ionides J, and Laue ED (2005). The CCPN data model for NMR spectroscopy: development of a software pipeline. Proteins 59, 687–696. [PubMed: 15815974]

Wang YY, Chang RB, Waters HN, McKemy DD, and Liman ER (2008). The nociceptor ion channel TRPA1 is potentiated and inactivated by permeating calcium ions. The Journal of biological chemistry 283, 32691–32703. [PubMed: 18775987]

Waterhouse AM, Martin DMA, Barton GJ, Procter JB, and Clamp M (2009). Jalview Version 2—a multiple sequence alignment editor and analysis workbench. Bioinformatics (Oxford, England) 25, 1189–1191.

Zhang C, Medzihradszky KF, Sánchez EE, Basbaum AI, and Julius D (2017). Lys49 myotoxin from the Brazilian lancehead pit viper elicits pain through regulated ATP release. Proceedings of the National Academy of Sciences of the United States of America 114, E2524–E2532. [PubMed: 28265084]

Author Manuscript Author Manuscript Author Manuscript Author Manuscript

Highlights

- WaTx is a cell-penetrating scorpion toxin targeting the TRPA1 ion channel
- WaTx and electrophiles converge on a shared intracellular ligand-binding domain
- WaTx binding stabilizes the TRPA1 open state and diminishes Ca^{2+}-permeability
- WaTx thus produces pain and pain hypersensitivity, but not neurogenic inflammation

Author Manuscript Author Manuscript Author Manuscript Author Manuscript

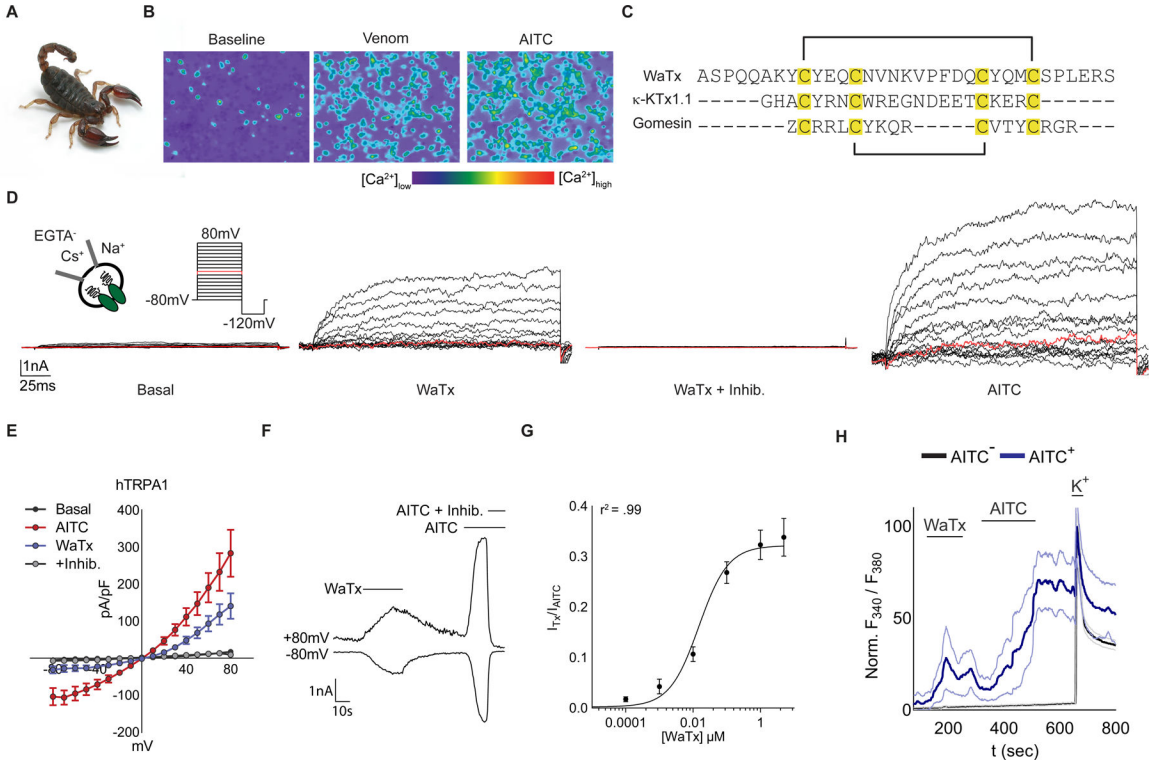

Figure 1. WaTx, a TRPA1-targeting peptide toxin from scorpion

(A) Australian Black Rock scorpion, *U. manicatus* (Museums Victoria, Creative Commons)

(B) Ca^{2+} responses in rat TRPA1-expressing HEK cells exposed to scorpion venom (~0.1 mg ml^{-1}), followed by AITC (333 μM).

(C) WaTx sequence, disulfide bonding configuration (black brackets), and manual alignment to example arachnid toxins with a 1–4, 2–3 disulfide bonding pattern, κ-KTx1.1, Hefutoxin (Srinivasan et al., 2002) and Gomesin (Silva et al., 2000). "Z" denotes pyroglutamate.

(D) Representative whole-cell recordings and, (E) derived current-voltage relationships for human (h) TRPA1 currents in HEK cells. WaTx (1 μM), WaTx + inhibitor (10 μM, A 967079), AITC (100 μM); $n = 5$ cells.

(F) Time-course of hTRPA1 responses in HEK cells. WaTx (250 nM), AITC (500 μM), and AITC + inhibitor (10 μM, A 967079); representative of $n = 3 – 10$ cells/treatment.

(G) WaTx dose-response relationship in HEK cells. Data fit by non-linear regression; $n = 3–26$ cells/dose.

(H) WaTx (5 μM) and AITC (50 μM) responses in cultured postnatal mouse trigeminal neurons. Representing $n = 3–10$ experiments.

All summary data, mean ± SEM. See also Figures S1, and S4; and Table S1

Author Manuscript Author Manuscript Author Manuscript Author Manuscript

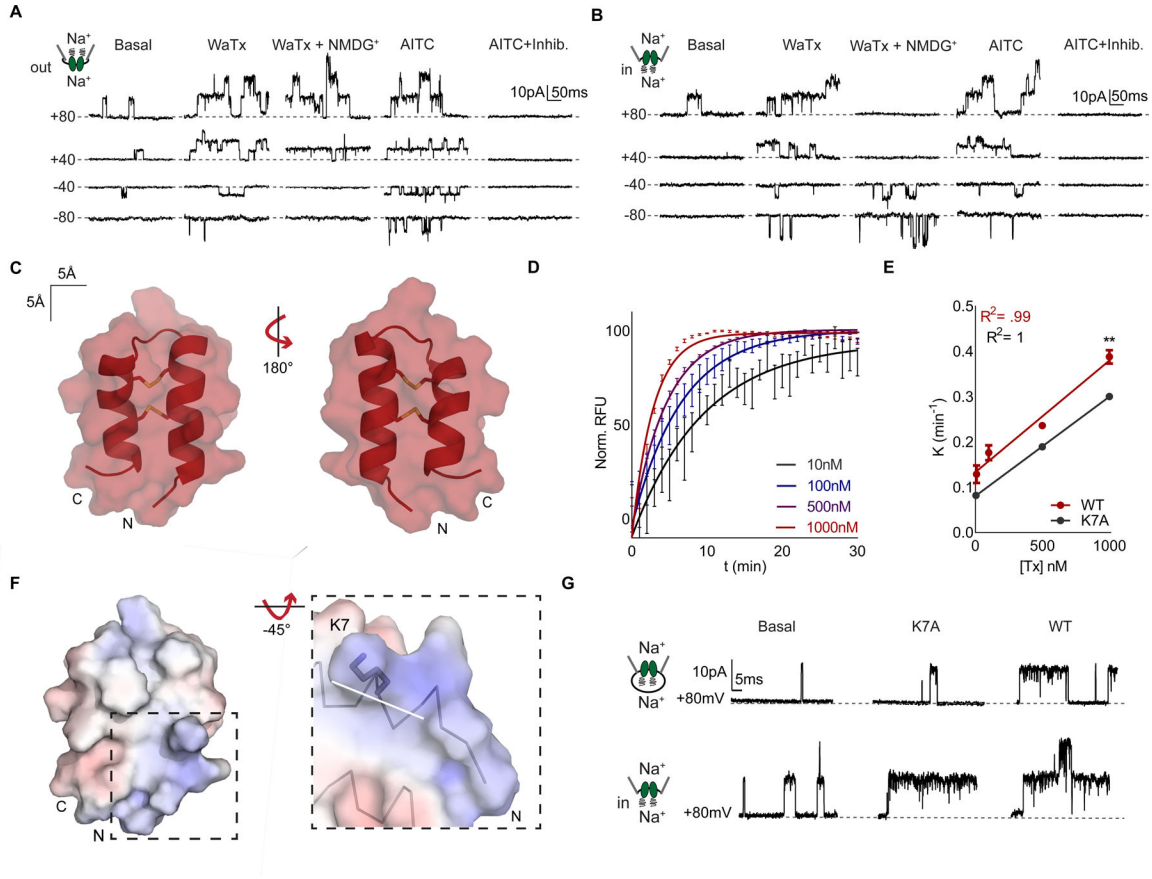

Figure 2. WaTx is a cell penetrating peptide

(A) Excised HEK cell patch recordings of TRPA1 single channels in outside-out (n = 10) or (B) inside-out, (n = 14) configuration in response to bath application of WaTx (100 nM), NMDG (150 mM), AITC (50 μM), and inhibitor (10 μM, A 967079). The orientation of the patch was confirmed by replacement of Na^+ with the impermeant cation, $NMDG^+$ and the identity of the single channels by application of the selective TRPA1 antagonist, A 967079 (Chen et al., 2011).

(C) Surface and cartoon representation of the closest-to-average (Kabsch RMSD = 0.355; mean Kabsch RMSD = 0.691) WaTx conformer (one of fifty) with disulfide bonds shown, determined by solution NMR spectroscopy. PDB ID: 6OFA.

(D, E) Kinetics and dose-dependence of toxin loading into soybean polar liposomes. Data fit by (D), nonlinear regression, one-phase exponential association and (E), linear regression. Unpaired, two-tailed Student's t-test, n = 6–8 wells/dose.

(F) WaTx electrostatic surface (Baker et al., 2001) contoured at ± 5 kT/e^-. Inset: WaTx N-terminus with dipole moment vector drawn in white (220 Debye, 1.65 Debye/atom (Felder et al., 2007)).

(G) Single-channel recordings of WT and K7A WaTx in (top) cell-attached and (bottom) inside-out HEK cell patch configuration; n = 5 inside-out and 12 cell-attached patches. All summary data, mean ± SEM. See also Figure S2 and Table S2

Author Manuscript Author Manuscript Author Manuscript Author Manuscript

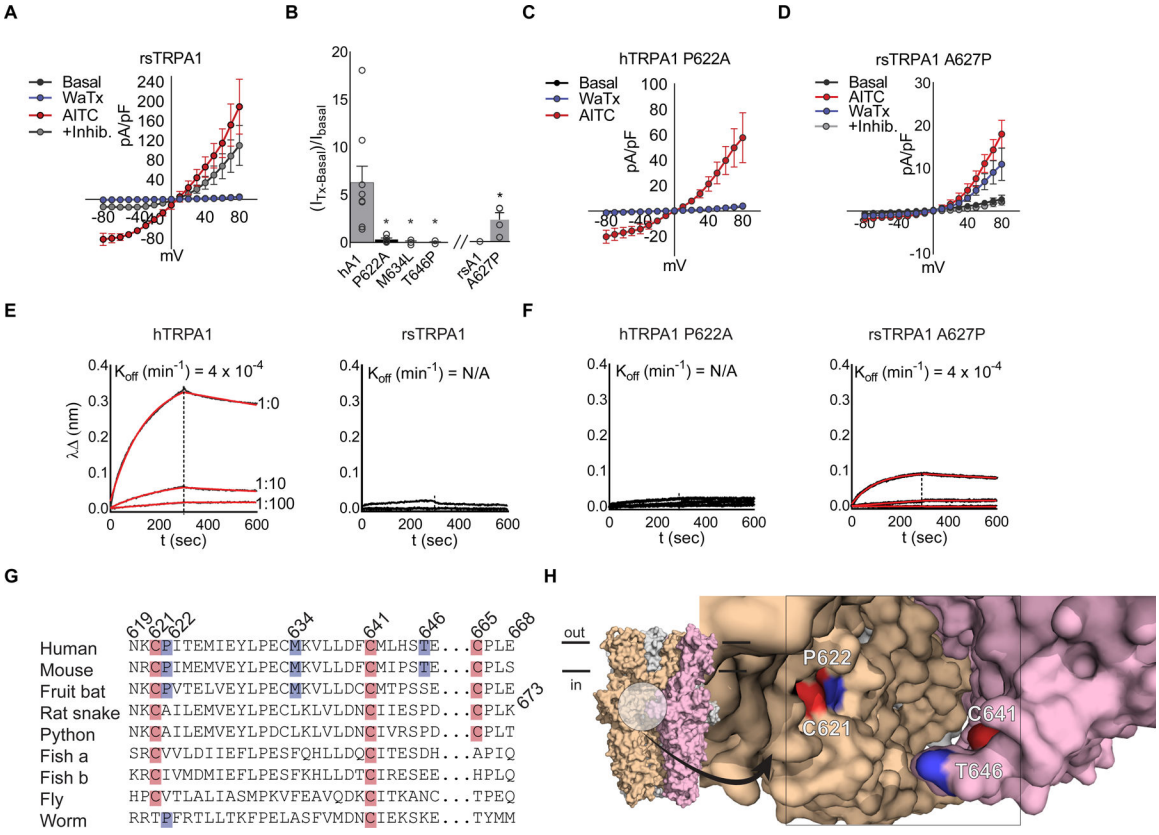

Figure 3. WaTx interacts directly with TRPA1's allosteric nexus

(A) Rat snake (rs) TRPA1 current-voltage relationships in transfected HEK cells. WaTx (100 nM), AITC (500 μM), AITC + inhibitor (50 μM, HC 030031); $n = 4$ cells. Note: inhibitor A 967079 is ineffective against rsTRPA1 while the selective TRPA1 inhibitor HC 030031 is effective (Banzawa et al., 2014; McNamara et al., 2007).

(B) WaTx-evoked whole cell currents for loss-of-function hTRPA1 mutants and gain-of-function rsTRPA1 mutant. WaTx treatments: 1 μM to hTRPA1 and 5 μM to rsTRPA1 constructs. One-Way ANOVA with *post-hoc* Holm-Sidak correction for multiple comparisons (hTRPA1 constructs) and unpaired two-tailed Student's *t*-test (rsTRPA1 constructs.). Recordings from transfected HEK cells; $n = 3–9$ cells/construct.

(C, D) Current-voltage relationships for hTRPA1 P622 mutants, which dictate species selectivity of TRPA1. Recordings from transfected HEK cells; $n = 4–5$ cells/treatment.

(E, F) Biolayer-interferometry derived sensorgrams depicting association of crude HEK cell membranes expressing TRPA1 to WaTx-coated sensors. Non-specific binding to mock-transfected membranes was subtracted, and resultant curves fit by nonlinear regression to a one-phase exponential association and dissociation model; Data are representative of $n = 3–6$ independent experiments/construct.

(G) Multiple-sequence alignment of TRPA1 orthologs and (H) proposed WaTx binding pocket mapped to the cryo-EM structure of human TRPA1 (PDB ID: 3J9P). Electrophile-reactive cysteines highlighted red; residues implicated in WaTx binding, blue.

All summary data, mean ± SEM. See also Figure S3.

Author Manuscript Author Manuscript Author Manuscript Author Manuscript

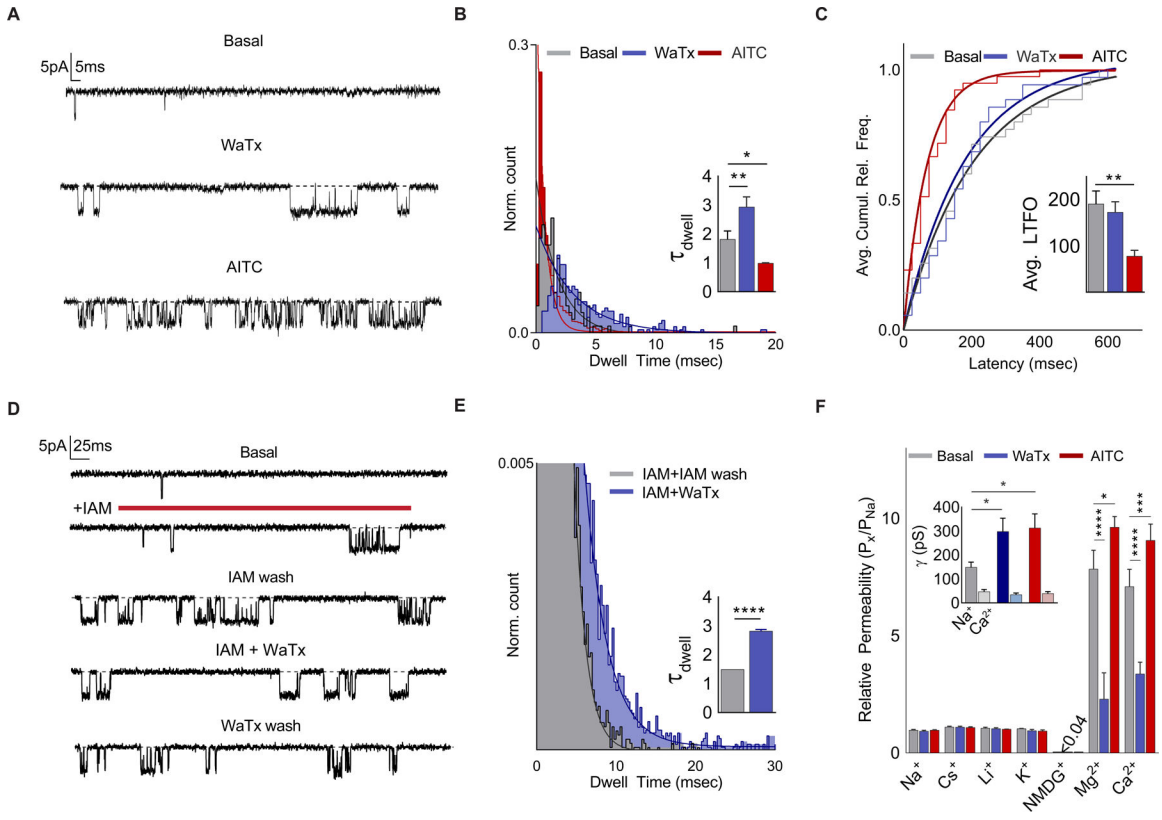

Figure 4. WaTx is a mode-specific gating modifier

(A-C) Inside-out HEK cell patch recordings (V_h = −40 mV) of spontaneous, WaTx (100 nM) or AITC (10 μM)-evoked TRPA1 openings, quantified with respect to (B), dwell time (n = 6–8 patches/treatment) and (C) latency to first opening (n = 13–14 patches/treatment). One-Way ANOVA with *post-hoc* Holm-Sidak correction for multiple comparisons.

(D) Inside-out HEK cell patch recordings (V_h = −40 mV) showing WaTx (1 μM) effect on a single, irreversibly activated (Iodoacetamide, 100 μM) TRPA1 channel (n = 9–11 patches/treatment), quantified with respect to (E) dwell time. Unpaired two-tailed Student's t-test.

(F) TRPA1 ionic selectivity and conductance for spontaneous, WaTx (100 nM)- or AITC (50 μM)-evoked openings (n = 3–7 HEK cell patches/condition). Two-way ANOVA with *post-hoc* Holm-Sidak correction.

All summary data, mean ± SEM. See also Figure S4.

Author Manuscript Author Manuscript Author Manuscript Author Manuscript

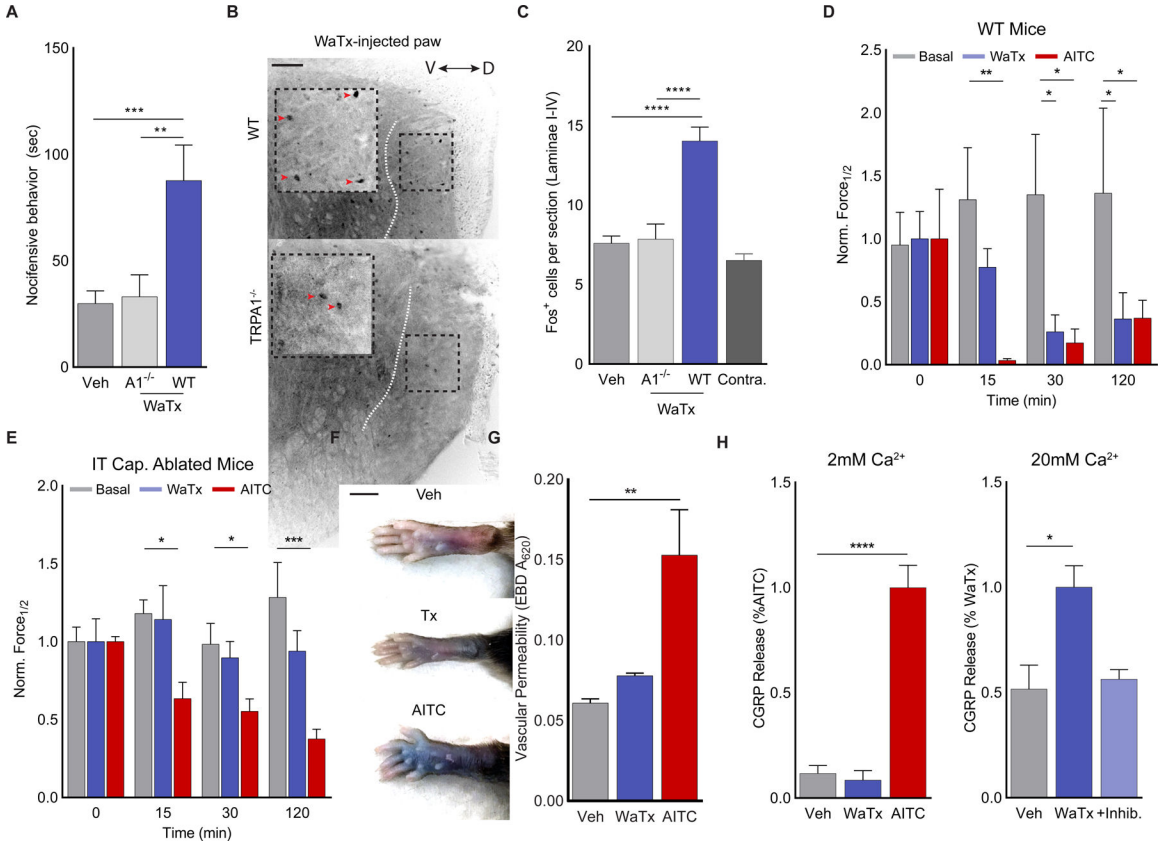

Figure 5. WaTx elicits TRPA1-dependent non-inflammatory pain

(A) WaTx-evoked nocifensive behavior in mice. One-way ANOVA with *post-hoc* Holm-Sidak correction for multiple comparisons; n = 12–20 mice/group.

(B, C) Induction of cFOS expression in the superficial laminae of the mouse spinal cord (dorsal to the dotted white line) after WaTx injection. Orientation of spinal cord along the dorsoventral axis indicated with bidirectional arrow. Inverted grayscale image with scale bar = 100 μm. One-way ANOVA with *post-hoc* Holm-Sidak correction for multiple comparisons; n = 22–39 sections/group.

(D, E) Timecourse and magnitude of mechanical allodynia onset in (D) wild-type (n = 8 animals/treatment) and (E) intrathecally capsaicin ablated mice (n = 6–8 mice/treatment) in response to vehicle, WaTx (100nM), or AITC injection (0.75% v/v in mineral oil). One-way ANOVA with *post-hoc* Holm-Sidak correction for multiple comparisons.

(F) Paw edema and (G) vascular permeability in mice after WaTx (100nM) or AITC (0.75% v/v in mineral oil) injection. One-way ANOVA with *post-hoc* Holm-Sidak correction for multiple comparisons; n = 4 mice/treatment. Scale bar: 5 mm.

(H) Measurements of CGRP release cultured neonatal rat trigeminal neurons under physiological (2mM) and high (20mM) extracellular Ca^{2+} conditions. Treatments: vehicle (PBS, pH 7.4), WaTx (10 μM), AITC (100 μM), and inhibitor A 967079 (10μM). One-Way ANOVA with *post-hoc* Holm-Sidak correction for multiple comparisons; n = 6–12 treatments/condition.

All summary data, mean ± SEM. See also Figure S5.

Author Manuscript Author Manuscript Author Manuscript Author Manuscript

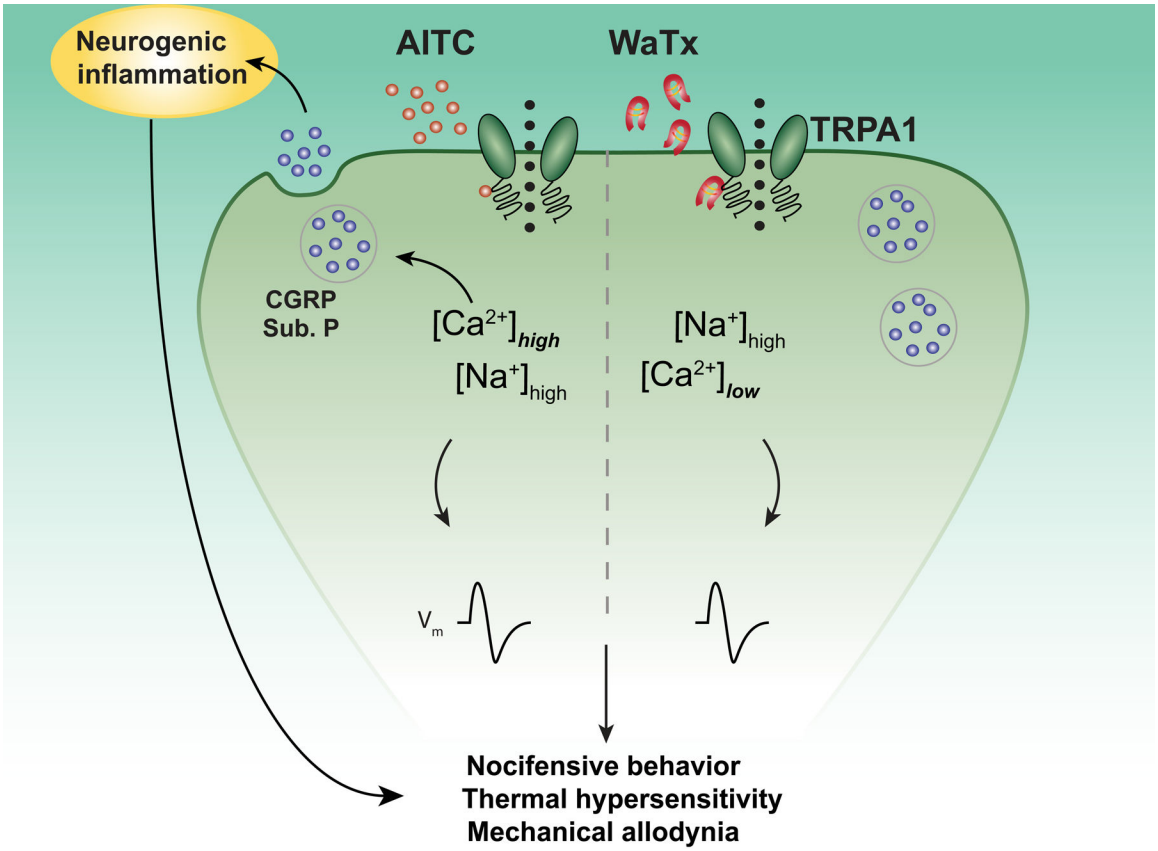

Figure 6. WaTx versus electrophile action at a sensory nerve terminal

Electrophilic irritants such as AITC act as membrane-permeable, covalent agonists for TRPA1, producing channel activation and neuronal depolarization; and, in turn, acute pain and subsequent hypersensitivities to noxious and innocuous stimuli. Concomitantly, electrophile activation produces robust Ca^{2+} entry, leading to Ca^{2+}-mediated release of CGRP from dense-core vesicles and consequent neurogenic inflammation. In contract, WaTx acts as a cell-penetrating, non-covalent gating modifier, producing prolonged spontaneous TRPA1 openings and, consequently, neuronal depolarization and subsequent hypersensitivities. However, WaTx also decreases the relative Ca^{2+}-permeability of TRPA1, forestalling sufficient Ca^{2+}-entry to produce measurable CGRP release and neurogenic inflammation.